

Separase-triggered apoptosis enforces minimal length of mitosis

<https://doi.org/10.1038/s41586-020-2187-y>

Susanne Hellmuth¹ & Olaf Stemmann¹✉

Received: 22 March 2019

Accepted: 10 February 2020

Published online: 08 April 2020

 Check for updates

Prolonged mitosis often results in apoptosis¹. Shortened mitosis causes tumorigenic aneuploidy, but it is unclear whether it also activates the apoptotic machinery². Separase, a cysteine protease and trigger of all eukaryotic anaphases, has a caspase-like catalytic domain but has not previously been associated with cell death^{3,4}. Here we show that human cells that enter mitosis with already active separase rapidly undergo death in mitosis owing to direct cleavage of anti-apoptotic MCL1 and BCL-XL by separase. Cleavage not only prevents MCL1 and BCL-XL from sequestering pro-apoptotic BAK, but also converts them into active promoters of death in mitosis. Our data strongly suggest that the deadliest cleavage fragment, the C-terminal half of MCL1, forms BAK/BAX-like pores in the mitochondrial outer membrane. MCL1 and BCL-XL are turned into separase substrates only upon phosphorylation by NEK2A. Early mitotic degradation of this kinase is therefore crucial for preventing apoptosis upon scheduled activation of separase in metaphase. Speeding up mitosis by abrogation of the spindle assembly checkpoint results in a temporal overlap of the enzymatic activities of NEK2A and separase and consequently in cell death. We propose that NEK2A and separase jointly check on spindle assembly checkpoint integrity and eliminate cells that are prone to chromosome missegregation owing to accelerated progression through early mitosis.

The intrinsic pathway of apoptosis is regulated by a balance between pro- and anti-apoptotic BCL2 family proteins that are hallmark of presence of one to four BCL2 homology (BH) domains⁵. Pore formation by homo-oligomerization of BAK and BAX leads to mitochondrial outer membrane permeabilization (MOMP) and release of cytochrome c and other apoptogenic factors from the intermembrane space. MOMP is counteracted by family members such as BCL2 itself, BCL2-like 1 (BCL-XL) and myeloid cell leukaemia 1 (MCL1). These proteins use a hydrophobic groove formed by their BH1–3 domains to sequester the BH3 domain of BAK/BAX and inhibit their self-interaction. BH3-only proteins such as BIM or BAD activate BAK/BAX either directly by transient interaction or indirectly by forcing BAK/BAX off anti-apoptotic BCL2 members through competition⁶. Intrinsic apoptosis in response to excessive cellular stress, such as DNA damage, is initiated by activation of BH3-only proteins, typically via upregulated transcription^{5,7}. Other triggers of intrinsic apoptosis are less well understood. Likewise, it remains unclear whether proteins other than BAK/BAX might also be able to form pores and contribute to MOMP.

Separase is the essential trigger protease of all eukaryotic anaphases⁴. Once activated in metaphase, it opens the DNA-embracing cohesin ring complex by cleavage of the kleisin subunit, thus resolving sister chromatid cohesion and enabling chromosome segregation. Separase contains a C-terminal caspase-like proteolytic domain³, but it has not been functionally linked to apoptosis. For most of the cell cycle, spindle assembly checkpoint (SAC) signalling ensures that human separase is held inactive by association with securin, SGO2–MAD2 or CDK1–cyclin B1^{8,9}. In response to improper attachment of kinetochores to spindle

microtubules, the SAC delays activation of separase and other late mitotic events, thereby giving the cell time for error correction^{2,10}. Hyperstimulation of the SAC by spindle toxins such as taxol (paclitaxel) prolongs mitosis¹¹. Conversely, SAC impairment results in shortened mitosis, chromosomal instability and tumorigenesis². While prolonged mitosis is known to result in death in mitosis (DiM) or mitotic slippage followed by apoptosis in interphase¹, it remains unstudied whether shortened mitosis might also trigger intrinsic apoptosis.

DiM upon premature separase activation

Both depletion of the cohesion-protecting factors SGO1 or securin and derepression of separase (by co-depletion of SGO2 and securin) result in premature sister chromatid separation^{9,12,13} (Extended Data Fig. 1a). This was followed by prolonged mitotic arrest of cells lacking SGO1 or securin, as previously described^{12,13}. However, cells lacking SGO2 and securin exhibited DiM as judged by cleavage of poly(ADP-ribose) polymerase (PARP) and fluorogenic caspase reporters (Extended Data Fig. 1b–h). DiM in cells depleted of SGO2 and securin was specific because it was suppressed by concomitant knockdown of separase (Extended Data Fig. 1g, h). Thus, premature activity of separase rather than premature sister chromatid separation represents an apoptotic stimulus.

MCL1 and BCL-XL are separase substrates

We speculated that MCL1 and BCL-XL could be relevant targets of separase in DiM because both (1) have previously been linked to apoptosis

¹Chair of Genetics, University of Bayreuth, Bayreuth, Germany. ✉e-mail: olaf.stemmann@uni-bayreuth.de

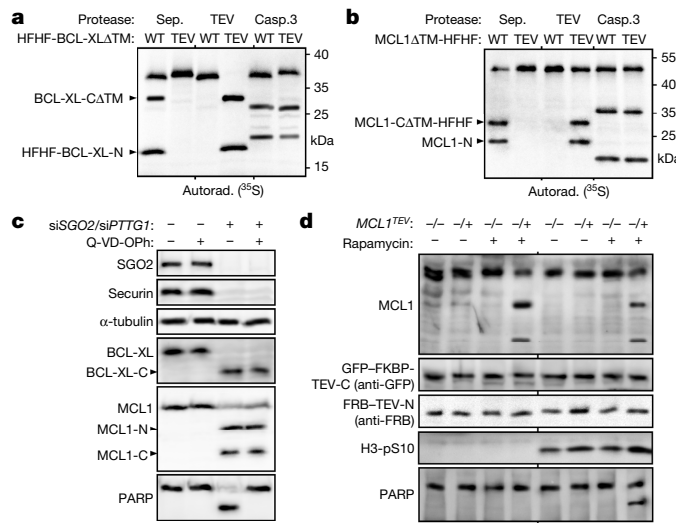


Fig. 1 | The pro-survival factors MCL1 and BCL-XL are separase substrates. **a, b,** Autoradiographies of in vitro cleavage assays in the presence of active NEK2A and ATP. WT, wild type; HFHF, His₆-Flag-His₆-Flag tag; ΔTM, transmembrane domain deleted. **c,** siRNA-transfected, taxol-arrested Hek293T cells were treated with Q-VD-OPh or mock-treated and analysed by immunoblotting. si $PTTG1$, securin depletion. **d,** Immunoblots of parental (−/−) and MCL1^{TEV} heterozygous (+/−) hTERT RPE1 cells after (+) or without (−) rapamycin-induced TEV protease complementation. H3-pS10, Ser10-phosphorylated histone H3 (mitotic marker).

after prolonged mitotic arrest^{14–17}; (2) have been reported to be cleaved by caspases^{18,19}; and (3) contain an ExxR motif that matches the consensus cleavage site of separase close to the caspase cleavage site(s). Indeed, human BCL-XL and MCL1 were cleaved in vitro not only by caspase 3 but also by separase, and the resulting fragments were clearly distinguishable in size (Fig. 1a, b). Replacing 31-ExxR-34 in BCL-XL and 173-ExxR-176 in MCL1 with tobacco etch virus (TEV)-protease cleavage sites required only a few amino acid exchanges (Extended Data Fig. 2a). This rendered both survival factors resistant to separase but susceptible to TEV protease, while leaving cleavage by caspase 3 unaffected (Fig. 1a, b). The proteolytic fragments that were generated by either separase or TEV protease exhibited identical mobilities in SDS-PAGE, thereby indicating that separase cleaves BCL-XL after Arg34 and MCL1 after Arg176. Various in vitro-expressed fragments were used as length standards to confirm the location of the cleavage site for MCL1 (Extended Data Fig. 2b). In mice, the ExxR motif is conserved in BCL-XL but has been replaced with DxxR in MCL1. Still, mouse MCL1 was readily cleaved by separase in vitro (Extended Data Fig. 2c). BCL-XL and MCL1 were also cleaved in human Hek293T, HeLa-K, HCT116, hTERT RPE1 and mouse NIH/3T3 cells during DiM triggered by RNA interference (RNAi) using small interfering RNAs (siRNAs) against SGO2 and PTTG1 (which encodes securin) (Extended Data Fig. 2d–g; see also below). Notably, these in vivo cleavages were mediated by separase rather than caspase because (1) Q-VD-OPh, a pan-specific caspase inhibitor, blocked cleavage of PARP but not of BCL-XL and MCL1 (Fig. 1c); (2) fragmentation was not detectable when the endogenous proteins were replaced by their separase-resistant but caspase-sensitive TEV variants (Extended Data Fig. 2d); and (3) MCL1 fragments from Hek293T cells lacking SGO2 and securin perfectly co-migrated with in vitro-expressed fragments comprising amino acids 1–176 (MCL1-N) and 177–350 (MCL1-C) (Extended Data Fig. 2f). In fact, we never observed caspase-dependent processing of MCL1 or BCL-XL in vivo, although this might be due to our focus on early stages of DiM. Using CRISPR–Cas9 gene editing in hTERT RPE1 cells, we replaced the separase cleavage site with a TEV protease cleavage site in one allele of MCL1. Upon activation of ‘split TEV protease’ by

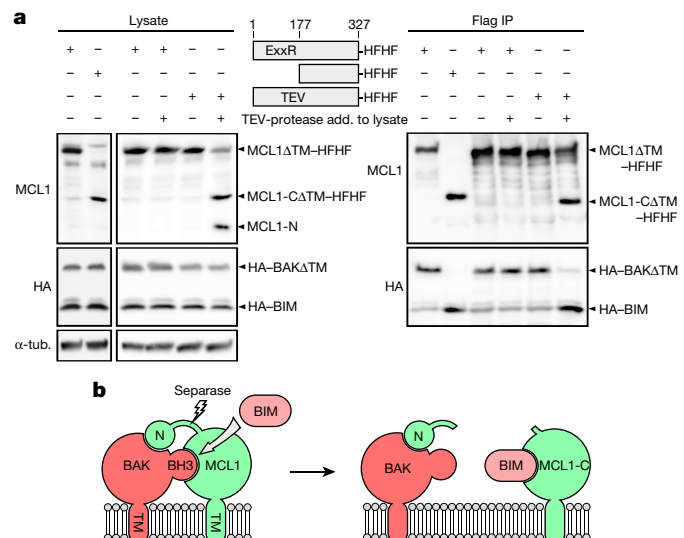


Fig. 2 | Cleavage of MCL1 by separase enables BH3-only proteins to liberate BAK. **a,** Immunoblots of (TEV protease supplemented, +) lysates and Flag immunoprecipitation of transfected, mitotic Hek293T cells expressing the indicated, C-terminally His₆-Flag-His₆-Flag (HFHF)-tagged MCL1 fragments together with HA-tagged BAK and BIM. **b,** Model of how separase inactivates MCL1.

rapamycin-induced complementation, half of endogenous MCL1 was cleaved, as expected (Fig. 1d). This was accompanied by considerable PARP cleavage, but only when the cells were in mitosis. Thus, MCL1 cleavage at position 176 is sufficient to initiate DiM during a prometaphase arrest.

Cleavage of MCL1 and BCL-XL liberates BAK

We investigated whether separase-dependent cleavage affected the interactions of MCL1 and BCL-XL with other BCL2 family members. To this end, we used Flag tags to affinity-purify MCL1 and the corresponding C-terminal separase cleavage fragment from transfected Hek293T cells and analysed them for association with co-expressed BAK relative to the BH3-only protein BIM. Whereas MCL1 preferentially interacted with BAK, as expected, MCL1-C bound only to BIM (Fig. 2a). An analogous experiment was conducted with BCL-XL but using BAD instead of BIM owing to the different binding preference of its C-terminal fragment (Extended Data Fig. 3a). Removal of the N-terminal 34 amino acids switched BCL-XL from binding BAK to binding BAD (Extended Data Fig. 3b). For MCL1, the exchange of binding partners upon cleavage was additionally recapitulated by addition of TEV protease to cell lysate containing the TEV variant of MCL1 (Fig. 2a). The BH4 domain of BCL2 contributes directly to BAX binding²⁰. Similarly, MCL1-N co-purified with BAK from transfected Hek293T cells (Extended Data Fig. 3c), showing that MCL1 contacts BAK not only via its hydrophobic groove but also via its N-terminal domain. We propose that cleavage by separase abolishes the cooperativity of binding, thereby enabling BH3-only proteins such as BIM to supersede BAK from the C-terminal fragment of MCL1 (Fig. 2b). Liberated BAK would then lead to MOMP.

MCL1-N and MCL1-C actively promote apoptosis

We made the counter-intuitive observation that DiM induced by siRNAs against SGO2 and PTTG1 was alleviated by co-depletion of MCL1 (Fig. 3a, b) and almost fully rescued by co-depletion of both MCL1 and BCL-XL (Extended Data Fig. 3d, e). While this showed that these two BCL2 family proteins are the crucial—if not the only—substrates of separase during DiM, it also suggested that the separase cleavage fragments of MCL1

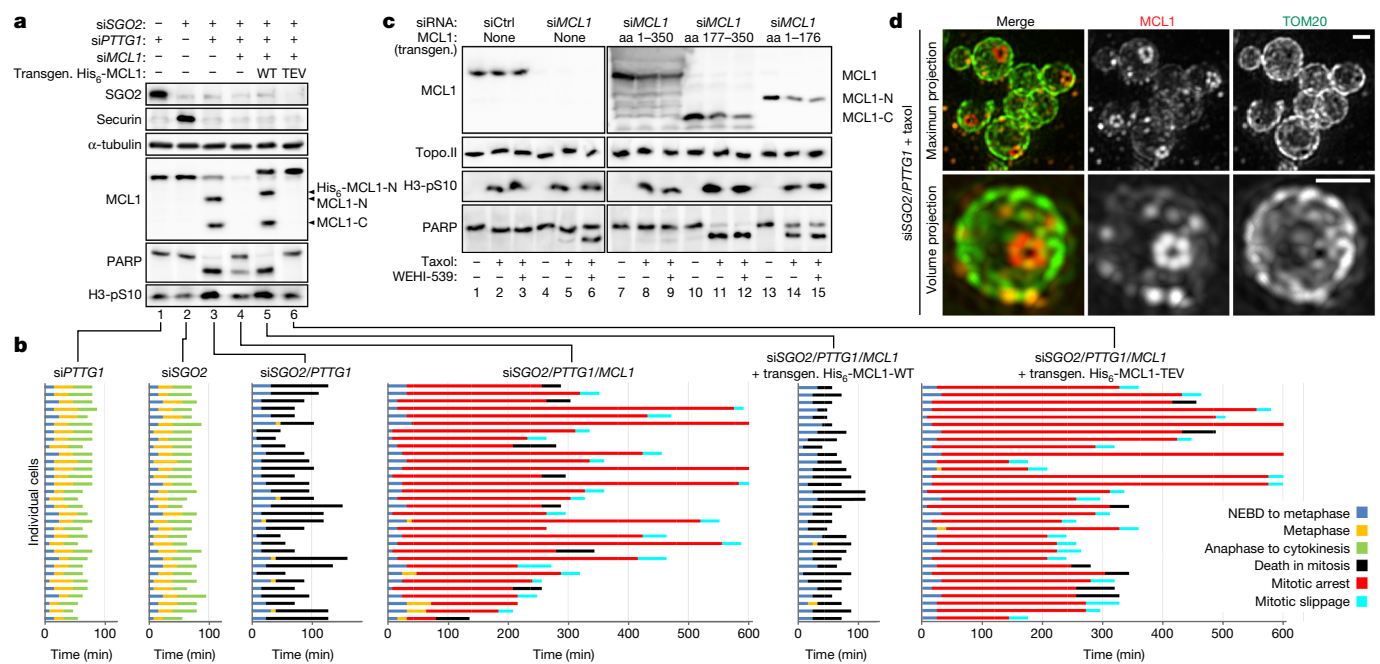


Fig. 3 | Both separase cleavage fragments of MCL1 are pro-apoptotic and MCL1-C forms macropores during late stages of DiM. **a, b,** HeLa-K cells transfected with the indicated siRNAs and expression plasmids were released from early S-phase arrest, supplemented with the DNA stain SiR-Hoechst and a fluorogenic caspase-3/7 reporter and analysed by immunoblotting (**a**; 10 h after release) and live cell imaging (**b**; cell fate profiles). **c,** Immunoblots of

MCL1- or control-depleted HeLa-K cells expressing transgenic full-length MCL1 or fragments thereof as indicated. **d,** Immunofluorescence 2D SIM of SGO2- and securin-depleted Hek293T cells undergoing DiM. Note the absence of the mitochondrial outer membrane marker TOM20 from the centres of MCL1 rings. Scale bars, 0.5 μm.

and BCL-XL are apoptotic. Consistent with this hypothesis, the mitigation of PARP cleavage by depletion of BCL-XL or MCL1 (Extended Data Fig. 2d, lanes 4–6) was reversed by expression of siRNA-resistant transgenic BCL-XL or MCL1 but not their separase-resistant TEV variants (lanes 7–10). Given the stronger effects of MCL1 depletion, we further studied its cleavage fragments individually. Full-length MCL1, MCL1-N or MCL1-C was expressed in Hek293T cells in which endogenous MCL1 (but not SGO2 or securin) was depleted by RNAi. Short-term absence of MCL1 caused very little apoptosis on its own but led to some cell death in conjunction with chemical inhibition of BCL-XL by WEHI-539 (Fig. 3c, lanes 5 and 6). This phenotype was rescued by transgenic full-length MCL1 (lane 9). Notably, expression of MCL1-N or MCL1-C resulted in PARP cleavage even in the absence of WEHI-539, with the C-terminal fragment having the stronger effect (lanes 11 and 14). PARP cleavage correlated with annexin V and propidium iodide staining as additional markers for apoptosis (Extended Data Fig. 3f, g). Induction of apoptosis by MCL1-N or MCL1-C did not occur in interphase but only in taxol-treated cultures (Fig. 3c, Extended Data Fig. 3f). Time-lapse microscopy further illustrated that HeLa-K cells expressing MCL1-N or MCL1-C also underwent DiM in the absence of spindle toxin (Extended Data Fig. 3h, i). Thus, separase-dependent cleavage not only extinguishes the pro-survival activity of MCL1 but also creates two fragments, each of which kills cells upon entry into mitosis without requiring prolonged mitotic arrest. Investigation of MCL1-N-induced apoptosis suggested that it promotes both liberation of BAK and separase-dependent cleavage of BCL-XL by a positive feedback mechanism (Extended Data Fig. 4).

MCL1-C kills by mitosis-specific MOMP

Interaction analyses of epitope-tagged forms of MCL1 revealed that MCL1-C exhibited homotypic interactions, whereas uncleaved, full-length MCL1 could associate neither with itself nor with MCL1-C (Extended Data Fig. 5a). Self-interaction of MCL1-C and its ability to

induce PARP cleavage were blocked by deletion of the transmembrane domain or presence of the BH3-mimicking MCL1-inhibitor A-1210477, which blocked not only binding of BAK to full-length MCL1 but also binding of BIM to MCL1-C (Extended Data Fig. 5b–d). Tandem affinity purification of co-expressed, differently tagged MCL1-C further revealed that homo-oligomerization and BIM binding are mutually exclusive (Extended Data Fig. 5d), which suggests that BIM interacts with MCL1-C only transiently and disengages upon MCL1-C self-interaction. These observations are reminiscent of the requirements for BAK/BAX-dependent MOMP^{21–23} and, thus, are consistent with pore formation by MCL1-C. Notably, homotypic MCL1-C interactions occurred only in extracts from mitotic, and not interphase, cells (Extended Data Fig. 5b); this is consistent with the finding that the pro-apoptotic effect of MCL1-C is cell-cycle-dependent. According to our hypothesis, separase-induced DiM should be delayed or diminished, but still occur, in the absence of BAK and BAX, whereas MCL1-C-induced DiM should be independent of them. Using time-resolved fractionation of chromatin and organelles, including mitochondria, from the cytosol followed by immunoblotting analyses, we compared parental HCT116 and *BAK*^{-/-} *BAX*^{-/-} double-knockout cells as they went synchronously from G2 through M-phase. Whereas the kinetics of MCL1-cleavage were indistinguishable in the absence of SGO2 and securin, the release of cytochrome c into the cytosol and PARP cleavage were delayed, but still occurred, in the absence of BAK and BAX (Extended Data Fig. 6a, b). In fact, PARP cleavage and accumulation of Ser139-phosphorylated histone H2A-X (γH2AX) in the absence of BAK and BAX were less affected during DiM induced by siRNAs against SGO2 and PTTG1 than during staurosporine-induced apoptosis²⁴ (Extended Data Fig. 6c). Notably, the timing and extent of cytochrome c release and PARP cleavage were the same in both cell lines when DiM was induced by MCL1-C expression (Extended Data Fig. 6d).

At later stages of intrinsic apoptosis, the mitochondrial network fragments into globular structures, and BAK and BAX form large rings and macropores within the outer membrane^{25–27}. Immunofluorescence

microscopy of MCL1 and the MOM protein TOM20 in taxol-arrested Hek293T cells showed that MCL1 and TOM20 colocalized during DiM, and this colocalization increased when the network dissolved into spheres (Extended Data Fig. 7a, b). Notably, 2D structural illumination microscopy (SIM) revealed the formation of large, typically 0.3- μ m rings by MCL1-C in SGO2- and securin-depleted cells undergoing DiM (Fig. 3d, Extended Data Fig. 7c). TOM20 appeared largely absent from the centre of the rings, suggesting that they represent macropores.

Phosphorylation might explain why the MOMP activity of MCL1-C is specific to mitosis. A candidate approach identified Thr301. Changing this residue to phosphorylation-mimicking Glu enabled MCL1-C to induce apoptosis also in interphase, whereas changing Thr301 to Ala abrogated the pro-apoptotic and self-interaction properties of MCL1-C (Extended Data Figs. 5d, 7d, e). The detection of affinity-purified MCL1-C by a phospho-Thr-specific antibody was limited to mitosis and abolished by the Thr301Ala mutation, suggesting that this position is phosphorylated in vivo (Extended Data Fig. 7d)—possibly by aurora B (Extended Data Fig. 7f, g). Existing structural information places Thr301 of MCL1 at the end of α -helix 6, and dimerization of the corresponding helix has been reported to be involved in homo-oligomerization of BAK^{28,29}. Sequence alignment implies that the Thr301-equivalent position is occupied by a Glu in BAX (Extended Data Fig. 7h). When we changed this constitutively negatively charged residue at position 146 to Ala, the pro-apoptotic function of BAX was abrogated, whereas changing it to Thr rendered BAX a largely mitosis-specific effector of cell death (Extended Data Fig. 7i). A salt bridge at the end of α -helix 6 might therefore be required for pore formation (Extended Data Fig. 7j) and explain why MCL1-C becomes pro-apoptotic only upon phosphorylation of Thr301 during mitosis, whereas MOMP by wild-type BAX is independent of the cell cycle.

Importance of phosphorylation by NEK2A

In unperturbed cells, MCL1 and BCL-XL are present at the onset of anaphase. The question arises of why then cells do not die when separase becomes active on schedule. Considering that cleavage of meiotic kleisin by separase requires its phosphorylation³⁰, we tested the effect of various kinases when first establishing MCL1 and BCL-XL cleavage by separase in vitro (Extended Data Fig. 8). These analyses revealed that cleavage of MCL1 by separase essentially requires NEK2A, while cleavage of BCL-XL was enabled by NEK2A and (less so) CDK1/2–cyclin A2 (note that NEK2A was included in Fig. 1a, b and Extended Data Figs. 2b, c, 4c). NEK2A and CDK1/2–cyclin A are special among mitotic kinases and APC/C substrates in that they are degraded early—that is, at a time when separase activation is still blocked by SAC signalling^{31,32}.

To identify phosphorylation sites within MCL1 and BCL-XL that are relevant for cleavage, we changed candidate serine and threonine residues to alanine or phosphorylation-mimicking acidic residues and screened corresponding variants in kinase and/or cleavage assays. These analyses revealed the following (Extended Data Fig. 9): (1) the NEK2A-dependent phosphorylation of Ser60 and Thr163 is essential for separase-dependent cleavage of MCL1, and phosphorylation of Ser159 further improves it. (2) NEK2A and CDK1/2–cyclin A2 phosphorylate Ser4 and Ser164, and Ser62, respectively, of BCL-XL to enable its cleavage by separase. (3) The phosphorylation-mimicking variants MCL1(S/T60,159,163D/Q) and BCL-XL(S4,62,164D) are cleaved by separase in the absence of kinases.

The above findings suggested that separase does not trigger DiM at anaphase onset merely because NEK2A (and cyclin A2) is absent by then and MCL1 and BCL-XL—owing to dephosphorylation—no longer represent separase substrates (Fig. 4a, top). As a corollary, any temporal overlap between the enzymatic activities of NEK2A and separase should cause DiM. Indeed, this explains why constitutive activity of separase causes early mitotic cell death and why knockdown of NEK2A largely suppressed DiM induced by siRNAs against SGO2 and

PTTG1 (Extended Data Fig. 1g, h). Extending the window of NEK2A activity until separase activation in anaphase should also cause DiM (Fig. 4a, middle). Live cell imaging of transfected HeLa-K cells revealed that overexpression of wild-type NEK2A was compatible with normal mitosis, whereas production of a C-terminally truncated, stabilized variant (Δ MR)³¹ triggered DiM, typically shortly after anaphase onset (Extended Data Figs. 3i, 10a). This was confirmed by time-resolved immunoprecipitation and western analysis of cells synchronously undergoing late mitosis. NEK2A- Δ MR-expressing and mock-treated populations both degraded cyclin B1 and securin and lost SGO2 from separase with similar kinetics (Extended Data Fig. 10b). However, only in NEK2A- Δ MR-containing cells did activation of separase coincide with cleavage of MCL1 and PARP. Consistent with MCL1 and BCL-XL being the relevant targets, apoptosis in anaphase was also triggered by expression of the constitutive separase substrates BCL-XL(S4,62,164D) or MCL1(S/T-60,159,163D/Q) instead of NEK2A- Δ MR (Extended Data Fig. 10c, d). Thus, NEK2A must be degraded in early mitosis to prevent separase from killing cells in anaphase.

Separase-induced DiM increases with MCL1

To investigate whether DiM in response to stabilization of NEK2A was graded with MCL1 dosage, we transfected siRNA or plasmids into Hek293T cells to express wild-type NEK2A or the Δ MR variant and, simultaneously, to reduce or increase the amount of MCL1. When transgenic NEK2A was wild-type and, hence, degraded upon entry into mitosis, or when NEK2A- Δ MR expression was combined with MCL1 depletion, cells showed no signs of apoptosis (Fig. 4b, Extended Data Fig. 11a–c). As seen before, NEK2A- Δ MR induced some DiM at endogenous levels of MCL1. However, annexin V staining and PARP cleavage increased with increasing levels of (transgene-encoded) MCL1 and cleavage fragments thereof. These data suggest that pharmacological inhibition of early mitotic NEK2A degradation should preferentially kill MCL1-overexpressing cells, which are a hallmark of many cancers³³.

A minimal duration of mitosis checkpoint

The SAC is active in each M-phase and chiefly determines its duration¹⁰. Abrogation of the SAC results in chromosomal instability owing to accelerated progression through mitosis². We investigated whether, under these conditions, separase might become active when NEK2A has not yet been fully degraded (Fig. 4a, bottom). When MAD2 and the SAC kinase BUBR1 were depleted by RNAi, HeLa-K cells that had been released from a thymidine arrest degraded securin and cyclin B1 earlier than control cells; this correlated with earlier auto-cleavage of separase, as expected (Fig. 4c). At the same time, degradation of NEK2A and the disappearance of a corresponding MCL1-S60 phosphorylation mark were delayed, which we attribute to competition by other substrates for the APC/C (Fig. 4c, Extended Data Fig. 11d). Notably, this was accompanied by cleavage of MCL1, BCL-XL and PARP and appearance of a sub-G1 peak in flow cytometry, which is another hallmark of apoptotic cells. As seen before, these phenotypes were largely suppressed by co-depletion of MCL1 and BCL-XL and fully suppressed by additional expression of separase-resistant TEV variants of MCL1 and BCL-XL, but re-installed by transfection with the corresponding wild-type transgenes. Cleavage of MCL1, BCL-XL and PARP also occurred upon individual depletion of MAD2 or BUBR1, albeit to lesser extent (Extended Data Fig. 11e). It also occurred in both mouse and human cells upon chemical inhibition of the SAC kinase MPS1 with reversine (Fig. 4d, Extended Data Fig. 11e). Thus, in mammalian cells SAC abrogation suffices to induce cleavage of MCL1 and BCL-XL by separase and consequent DiM. A corollary is that the few existing SAC-deficient tumour cell lines (unless slowed in mitotic progression

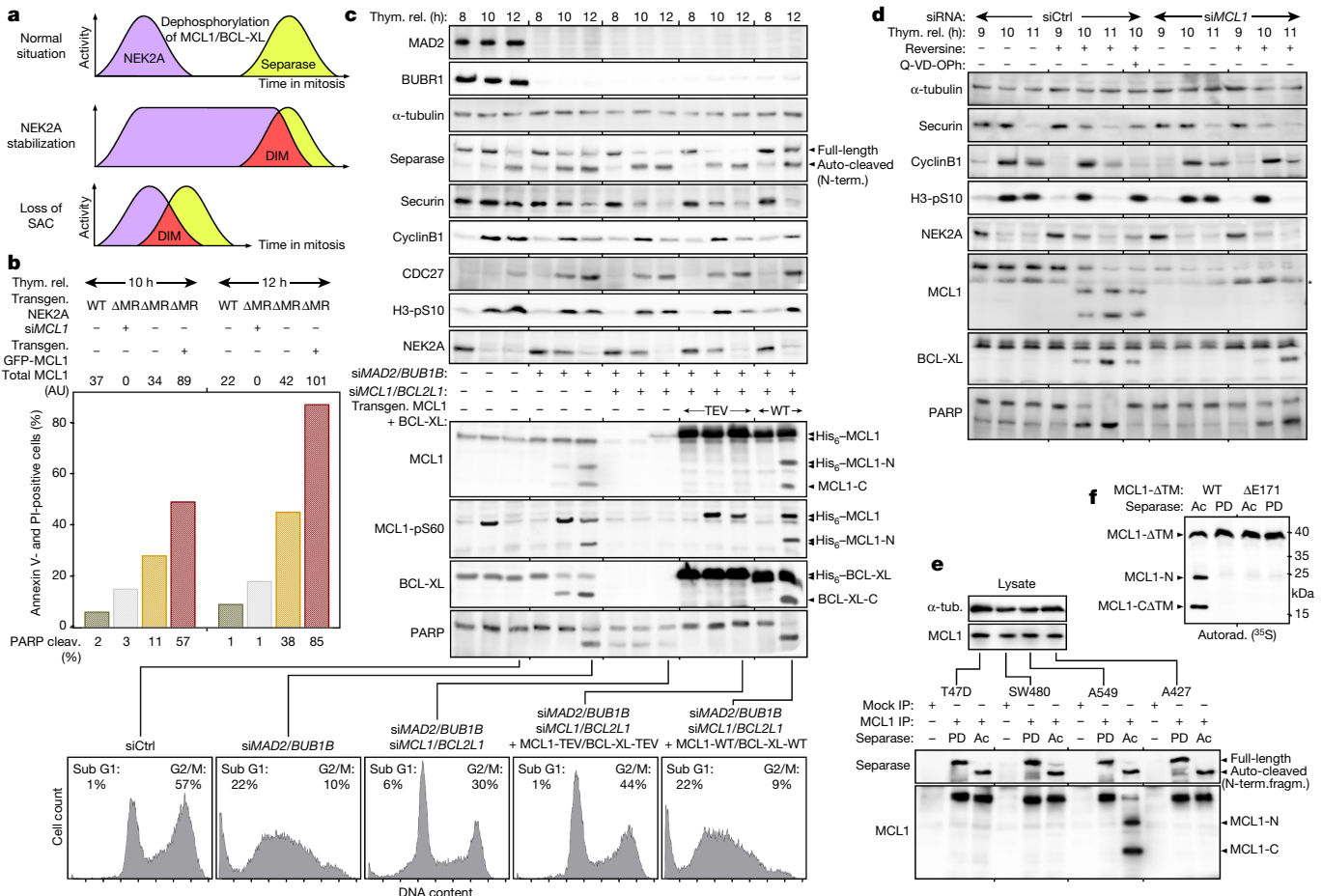


Fig. 4 | DiM due to simultaneous activity of NEK2A and separase is graded by MCL1 level and triggered by SAC deficiency. a, Both prolonged activity of NEK2A (middle) and speeded-up mitosis due to SAC deficiency (bottom) cause DiM. **b,** Fluorescence microscopic quantification of annexin V- and propidium iodide (PI)-positive Hek293T cells transfected with siMCL1 and expression plasmids for GFP-MCL1 and NEK2A-WT or NEK2A-ΔMR, as indicated, and released for 10–12 h from thymidine arrest (thy. rel.). Expression of MCL1 and degree of PARP cleavage were quantified by densitometry of immunoblots (Extended Data Fig. 11b). **c,** HeLa-K cells transfected with the indicated siRNAs

and expression plasmids were released from thymidine arrest and analysed by immunoblotting and propidium iodide staining with flow cytometry 8–12 h thereafter. siBUB1A, BUBR1 depletion; siBCL2L1, BCL-XL depletion. **d,** Time-resolved immunoblots of NIH/3T3 cells transfected with indicated siRNAs, pre-synchronized with thymidine, and treated with Q-VD-OPh and/or reversine, undergoing mitosis. Asterisk, nonspecific band. **e,** Immunoblots of lysates and NEK2A/separase-treated Mcl1 immunoprecipitations from the indicated cell lines. **f,** Autoradiograph of in vitro-expressed, NEK2A/separase-treated ³⁵S-MCL1-WT and ³⁵S-MCL1-ΔE171.

by SAC-independent means³⁴) should have found a way to avoid cleavage of MCL1 and BCL-XL. We immunoprecipitated MCL1 from four cancer cell lines: partially SAC-compromised SW480, SAC deficient T47D and A427 and, as a control, SAC-proficient A549 cells^{11,35,36}. Notably, only MCL1 from A549 cells was cleaved upon incubation with NEK2A and separase (Fig. 4e). It is unclear how MCL1 from the other three cell lines is rendered separase-resistant, but it is not due to the mere absence of p53 (Extended Data Fig. 11f). Cancer-associated MCL1 variants seem to be rare. However, of the few catalogued in the Catalogue of Somatic Mutations in Cancer (COSMIC) database³⁷, deletion of Glu171 is by far the most abundant one, being identified ten times in six studies. Although it leaves the ExxR motif intact, unexpectedly, this mutation renders MCL1 resistant to separase (Fig. 4f).

Conclusion

In most cases studied, the intrinsic pathway of apoptosis is triggered by transcriptional upregulation of BH3-only protein expression^{5,7}. Here, we describe a mechanism of DiM, which is probably conserved in vertebrates (Extended Data Fig. 12) and consists of separase-dependent

cleavage of MCL1 and BCL-XL and their concurrent transformation from pro-survival into mitosis-specific pro-apoptotic factors. Our results strongly suggest that the deadliest fragment, MCL1-C, permeabilizes the mitochondrial outer membrane by forming pores. Because separase-dependent cleavage of BCL-XL is also sufficient for DiM, the same might be true of BCL-XL-C. Degradation of MCL1 was causally linked to apoptosis upon mitotic arrest, but exactly how MCL1 is removed remains unknown^{15,16}. Although we have not done so here, it will therefore be interesting to investigate whether MCL1 somehow becomes phosphorylated and separase-activated during prolonged mitosis. Here we studied shortened mitosis. Our results show that abrogation of SAC results in DiM owing to simultaneous activity of NEK2A and separase (Fig. 4a, bottom). We propose that NEK2A and separase form a surveillance mechanism that eliminates SAC-deficient cells that would otherwise be doomed to massive chromosomal instability and aneuploidy, thereby ensuring the survival of cells with the correct length of M-phase and protecting the organism from tumorigenesis. This ‘minimal duration of early mitosis checkpoint’ (DMC) might explain why mutational inactivation of SAC genes in cancer is rare^{35,38}.

Online content

Any methods, additional references, Nature Research reporting summaries, source data, extended data, supplementary information, acknowledgements, peer review information; details of author contributions and competing interests; and statements of data and code availability are available at <https://doi.org/10.1038/s41586-020-2187-y>.

1. Gascoigne, K. E. & Taylor, S. S. Cancer cells display profound intra- and interline variation following prolonged exposure to antimitotic drugs. *Cancer Cell* **14**, 111–122 (2008).
2. Michel, L. S. et al. MAD2 haplo-insufficiency causes premature anaphase and chromosome instability in mammalian cells. *Nature* **409**, 355–359 (2001).
3. Lin, Z., Luo, X. & Yu, H. Structural basis of cohesin cleavage by separase. *Nature* **532**, 131–134 (2016).
4. Wirth, K. G. et al. Separase: a universal trigger for sister chromatid disjunction but not chromosome cycle progression. *J. Cell Biol.* **172**, 847–860 (2006).
5. Galluzzi, L. et al. Molecular mechanisms of cell death: recommendations of the Nomenclature Committee on Cell Death 2018. *Cell Death Differ.* **25**, 486–541 (2018).
6. Letai, A. et al. Distinct BH3 domains either sensitize or activate mitochondrial apoptosis, serving as prototype cancer therapeutics. *Cancer Cell* **2**, 183–192 (2002).
7. Villunger, A. et al. p53- and drug-induced apoptotic responses mediated by BH3-only proteins puma and noxa. *Science* **302**, 1036–1038 (2003).
8. Kamenz, J. & Hauf, S. Time to split up: dynamics of chromosome separation. *Trends Cell Biol.* **27**, 42–54 (2017).
9. Hellmuth, S. et al. Securin-independent regulation of separase by checkpoint-induced shugoshin-MAD2. *Nature* <https://doi.org/10.1038/s41586-020-2182-3> (2020).
10. Taylor, S. S. & McKeon, F. Kinetochore localization of murine Bub1 is required for normal mitotic timing and checkpoint response to spindle damage. *Cell* **89**, 727–735 (1997).
11. Li, Y. & Ben Ezra, R. Identification of a human mitotic checkpoint gene: hsMAD2. *Science* **274**, 246–248 (1996).
12. Rankin, S., Ayad, N. G. & Kirschner, M. W. Sororin, a substrate of the anaphase-promoting complex, is required for sister chromatid cohesion in vertebrates. *Mol. Cell* **18**, 185–200 (2005).
13. Tang, Z., Sun, Y., Harley, S. E., Zou, H. & Yu, H. Human Bub1 protects centromeric sister-chromatid cohesion through Shugoshin during mitosis. *Proc. Natl Acad. Sci. USA* **101**, 18012–18017 (2004).
14. Bennett, A. et al. Inhibition of Bcl-xL sensitizes cells to mitotic blockers, but not mitotic drivers. *Open Biol.* **6**, 160134 (2016).
15. Haschka, M. D. et al. The NOXA-MCL1-BIM axis defines lifespan on extended mitotic arrest. *Nat. Commun.* **6**, 6891 (2015).
16. Sloss, O., Topham, C., Diez, M. & Taylor, S. Mcl-1 dynamics influence mitotic slippage and death in mitosis. *Oncotarget* **7**, 5176–5192 (2016).
17. Topham, C. et al. MYC is a major determinant of mitotic cell fate. *Cancer Cell* **28**, 129–140 (2015).
18. Clem, R. J. et al. Modulation of cell death by Bcl-XL through caspase interaction. *Proc. Natl Acad. Sci. USA* **95**, 554–559 (1998).
19. Michels, J. et al. Mcl-1 is required for Akata6 B-lymphoma cell survival and is converted to a cell death molecule by efficient caspase-mediated cleavage. *Oncogene* **23**, 4818–4827 (2004).
20. Barclay, L. A. et al. Inhibition of pro-apoptotic BAX by a noncanonical interaction mechanism. *Mol. Cell* **57**, 873–886 (2015).
21. Brouwer, J. M. et al. Conversion of Bim-BH3 from activator to inhibitor of Bak through structure-based design. *Mol. Cell* **68**, 659–672.e659 (2017).
22. Czabotar, P. E. et al. Bax crystal structures reveal how BH3 domains activate Bax and nucleate its oligomerization to induce apoptosis. *Cell* **152**, 519–531 (2013).
23. Dai, H. et al. Transient binding of an activator BH3 domain to the Bak BH3-binding groove initiates Bak oligomerization. *J. Cell Biol.* **194**, 39–48 (2011).
24. Wang, C. & Youle, R. J. Predominant requirement of Bak for apoptosis in HCT116 cells is determined by Mcl-1's inhibitory effect on Bak. *Oncogene* **31**, 3177–3189 (2012).
25. Große, L. et al. Bax assembles into large ring-like structures remodeling the mitochondrial outer membrane in apoptosis. *EMBO J.* **35**, 402–413 (2016).
26. Salvador-Gallego, R. et al. Bax assembly into rings and arcs in apoptotic mitochondria is linked to membrane pores. *EMBO J.* **35**, 389–401 (2016).
27. McArthur, K. et al. BAK/BAX macropores facilitate mitochondrial herniation and mtDNA efflux during apoptosis. *Science* **359**, eaao6047 (2018).
28. Day, C. L. et al. Solution structure of prosurvival Mcl-1 and characterization of its binding by proapoptotic BH3-only ligands. *J. Biol. Chem.* **280**, 4738–4744 (2005).
29. Dewson, G. et al. Bak activation for apoptosis involves oligomerization of dimers via their a6 helices. *Mol. Cell* **36**, 696–703 (2009).
30. Kudo, N. R. et al. Role of cleavage by separase of the Rec8 kleisin subunit of cohesin during mammalian meiosis I. *J. Cell Sci.* **122**, 2686–2698 (2009).
31. Hayes, M. J. et al. Early mitotic degradation of Nek2A depends on Cdc20-independent interaction with the APC/C. *Nat. Cell Biol.* **8**, 607–614 (2006).
32. Wolthuis, R. et al. Cdc20 and Cks direct the spindle checkpoint-independent destruction of cyclin A. *Mol. Cell* **30**, 290–302 (2008).
33. Beroukhim, R. et al. The landscape of somatic copy-number alteration across human cancers. *Nature* **463**, 899–905 (2010).
34. Wild, T. et al. The spindle assembly checkpoint is not essential for viability of human cells with genetically lowered APC/C activity. *Cell Rep.* **14**, 1829–1840 (2016).
35. Tighe, A., Johnson, V. L., Albertella, M. & Taylor, S. S. Aneuploid colon cancer cells have a robust spindle checkpoint. *EMBO Rep.* **2**, 609–614 (2001).
36. Weitzel, D. H. & Vandré, D. D. Differential spindle assembly checkpoint response in human lung adenocarcinoma cells. *Cell Tissue Res.* **300**, 57–65 (2000).
37. Bamford, S. et al. The COSMIC (Catalogue of Somatic Mutations in Cancer) database and website. *Br. J. Cancer* **91**, 355–358 (2004).
38. Hernando, E. et al. Molecular analyses of the mitotic checkpoint components hsMAD2, hBUB1 and hBUB3 in human cancer. *Int. J. Cancer* **95**, 223–227 (2001).

Publisher's note Springer Nature remains neutral with regard to jurisdictional claims in published maps and institutional affiliations.

© The Author(s), under exclusive licence to Springer Nature Limited 2020

Methods

Antibodies

Antibodies generated within this study were raised and purified as described⁹. The following antibodies were used for immunoblotting and immunofluorescence microscopy (IFM): Rabbit anti-separase³⁹, rabbit anti-sororin⁴⁰, rabbit anti-PIN1⁴¹, goat anti-CDC27⁴², mouse anti-GFP⁴³, mouse anti-Flag (1:2,000; Sigma-Aldrich, M2), rabbit anti-SGO2 (1:1,000; Bethyl, A301-262A), rabbit or guinea pig anti-SGO2 (1.5 µg/ml; anti-DVPPRESHSHSDQSSKC), rabbit anti-SGO1 (1:500; Abcam, ab21633), mouse anti-securin (1:1,000; MBL, DCS-280), rabbit anti-phosphoSer10-histone H3 ('H3-pS10'; 1:1,000; Millipore, 06-570), mouse anti-cyclin B1 (1:1,000; Millipore, 05-373), rabbit anti-cleaved caspase 3 (Asp175; 1:1,000; Cell Signaling, 5A1E), rabbit anti-BCL-XL (1:1,000; Cell Signaling, 2762), mouse anti-MCL1 (1:800; BioLegend, W16014A), guinea-pig anti-MCL1 (0.75 µg/ml; for IFM 1.5 µg/ml; raised against amino acids 1–327 (ΔTM) of human MCL1), guinea-pig anti-phosphoSer10-MCL1 ('MCL1-pS60'; 0.5 µg/ml; for IFM 1 µg/ml; anti-CVIGGpSAGA, liberated from reactivity towards CVIGGSAGA), anti-TOM20 (1:500; Santa-Cruz Biotechnology, F10), mouse anti-cytochrome c (1:1,000; BD Pharmingen, 7H8.2C12), mouse anti-Bubr1 (1:1,000; BD Transduction Laboratories, clone 9), rabbit anti-BAX (1:1,000; Abcam, ab32503), rabbit anti-BAK (1:1,000; Abcam, ab32371), rabbit anti-MAD2 (1:1,000; Bethyl, A300-300A), rabbit anti-PARP (1:800; Cell Signaling, 46D11), mouse anti-PARP (1:1000; Calbiochem, AM30), anti-MBP monoclonal (1:1,000; NEB Biolabs, E8038S, HRP-conjugated), mouse anti-NEK2 (1:600; BD Transduction Laboratories, clone 20), mouse anti-RGS-His₆ (1:1,000; Qiagen 34610), rabbit anti-phosphoSer139-histone H2A.X ('γH2AX'; 1:5,000; Millipore, EP854(2)Y), mouse anti-topoisomerase IIα (1:1,000; Enzo Life Sciences, 1C5), mouse anti-cyclin A2 (1:200; Santa Cruz Biotechnology, 46B11), rat anti-HA (1:2,000; Roche, 3F10) and mouse anti-α-tubulin (hybridoma supernatant 1:200; DSHB, 12G10). Nonspecific rabbit, mouse and guinea pig IgGs were from Sigma-Aldrich. For immunoprecipitation experiments, the following affinity matrices and antibodies were used: mouse anti-Flag agarose (Sigma-Aldrich, M2), rat anti-HA agarose (Roche, clone 3F10), anti-GFP nanobody covalently coupled to NHS-agarose (GE Healthcare), mouse anti-RGS-His₆ or guinea pig anti-MCL1 coupled to protein G sepharose (GE Healthcare) and rabbit anti-BCL-XL coupled to protein A sepharose (GE Healthcare). For non-covalent coupling of antibodies, 10 µl of the respective matrix was rotated with 2–5 µg antibody in the presence of 1% w/v BSA (Roth) for 90 min at room temperature and then washed three times. Secondary antibodies for immunoblotting were horseradish peroxidase (HRP)-conjugated goat anti-rabbit, anti-mouse and anti-guinea pig IgGs (Sigma-Aldrich, all used at 1:20,000). The following secondary antibodies were used for IFM (all 1:500): Cy3 donkey anti-guinea pig IgG, Cy5 goat anti-mouse IgG (both Jackson ImmunoResearch Laboratories), Alexa Fluor 488 goat anti-mouse IgG (Invitrogen). Antisera against mouse SGO2 and mouse securin were gifts from A. M. Pendás.

Cell lines and plasmids

HeLa-K, Hek293T, hTERT RPE-1, HCT116, HCT116 BAK^{-/-}, BAX^{-/-}, HCT116 TP53^{-/-}, SW480, and NIH/3T3 cells were cultured in Dulbecco's modified Eagle's medium (DMEM) (Biowest), T-47D cells in RPMI-1640 (Biowest) and A427 and A549 cells in essential minimum Eagle's medium (EMEM) (Roth). All media were supplemented with 10% heat-inactivated fetal calf serum (FCS) (Sigma-Aldrich). Cells were cultured at 37 °C in 5% CO₂. *Xenopus laevis* S3 cells were grown at 27 °C under atmospheric CO₂ in 70% Leibovitz's L-15 medium (Gibco) supplemented with 1% Glutamax (Gibco) and 10% heat-inactivated FCS. *MCL1* (NM_021960) was PCR-cloned from human testis cDNA (Clontech), *BCL-XL* (*BCL2L1*, NM_138578), *BAK1* (*BCL2L7*, NM_001188), *BIM* (*BCL2L11*, NM_001204106) and *BAD* (*BCL2L8*, NM_032989) were PCR-cloned from self-made HeLa cell cDNA. *MCL1* from *X. laevis* (NP_001131055), *Xenopus tropicalis*

(XP_002935512) and *Danio rerio* (NP_571674) were PCR-cloned from self-made oocyte cDNA, zygote cDNA (a gift from C. Niehrs) and 72-h embryos (a gift from P. Braaker), respectively. Details about the resulting plasmids and derivatives thereof are available upon request. The ZipGFP plasmid was a gift from X. Shu (Addgene plasmid #81241)⁴⁴. For transient expression of proteins, Hek293T, HeLa-K or hTERT RPE-1 cells were transfected with corresponding pCS2- or pcDNAS-based plasmids using a calcium phosphate-based method or Lipofectamine 2000 (Invitrogen) according to the manufacturer's protocol. *X. laevis* S3 cells were transfected using PEI (Polysciences; 3 µl of 1 µg/µl per 1 µg DNA). *MCL1*^{+/TEV} hTERT RPE1 cells were generated using the co-CRISPR approach⁴⁵ with 0.8 µM ouabain octahydrate (Sigma) 72 h after transfection with 30 pmol ssODN *MCL1*^{TEV} (5'-GCTGGAGTTGGTCGGGGAAATC TGTTATAAACACCACTACCGACGGGTCACTACCCTCGACGCCGCCGC AGCAGAGGAGGAGGAGGACGAGAACTTGTACTTCCAGTCGCTCCAGA TTATCTCTCGGTACCTTCGGGAGC-3'), 10 pmol ssODN *ATP1A1* and 1 µg eSpCas9_ATP1A1_G3_Dual_sgRNA (a gift from Y. Doyon, Addgene plasmid #86613) encoding the corresponding sgRNA for *MCL1*^{TEV} (5'- CGAGTTGTACCGGCAGTCGC-3'). Ouabain-resistant clones were screened by PCR with oligonucleotides (fwd: 5'-GAGTTC GCTGGGCCACCCCGTAGGACT-3', rev: 5'-GGGAGTGAGGCCTGG CGATTAAATGAACCCCCTT-3') and the resulting 871-bp fragment was further analysed for the presence of a Xho1 site.

Cell treatments

For synchronization in early S-phase, human and frog cells were treated with 2 mM thymidine (Sigma-Aldrich) for 20 h. Upon release/wash-out, cells entered mitosis within 8–10 h. Synchronization of cells in prometaphase was done by addition of taxol (LC Laboratories) to 0.2 µg/ml 6 h after release from thymidine block. G2 arrest was achieved by addition of 10 µM RO-3306 (Santa-Cruz Biotechnology) 4 h after release from thymidine arrest for 6–10 h. For release from G2 arrest, cells were trypsinized, washed 5× with fresh medium and reseeded for the indicated incubation times. To inhibit MCL1, BCL-XL, caspases or MPS1 kinase, cells were supplemented with A-1210477 (2.5 µM, Abcam), WEHI-539 (0.5 µM, Cayman Chemicals), Q-VD-OPh (20 µM, BD Pharmingen) or reversine (1 or 5 µM, Cayman Chemicals), respectively, at the time of taxol addition and incubated for 6 h. To assess apoptosis in interphase, cells were arrested with thymidine for 20 h together with simultaneous transfection of corresponding plasmids or siRNA, released for 15 h, re-supplemented with thymidine and analysed 10 h thereafter. To assess apoptosis in mitosis, cells were transfected 10–12 h before thymidine addition, released and treated with taxol as described above, and collected when morphological signs of apoptosis first became visible (typically 10–13 h after thymidine wash-out). When studying depletion of MCL1 and BCL-XL without separase deregulation, the taxol arrest was prolonged to 12 h before cells were analysed. As control, cells were treated with 1 µM staurosporine (Abcam) for 8–12 h. To address DiM in SAC-abrogated HeLa-K cells, the corresponding plasmids were transfected first. Ten hours later, siRNA was transfected. Thymidine was added 14 h thereafter. (In the case of NIH/3T3 cells, thymidine (4 mM) was added immediately after siRNA transfection and washed away 18 h thereafter. This was followed by a second thymidine block 10 h later.) After 20 h, cells were released, re-seeded, supplemented with reversine (5 µM unless stated otherwise) and incubated for the indicated times without addition of taxol. For the 'taxol-ZM override' experiments, taxol-arrested HeLa-K cells were collected by shake-off and released for the indicated times by replating into medium supplemented with ZM 447439 (5 µM, Tocris Biosciences), taxol (0.2 µg/ml) and cycloheximide (30 µg/ml, Sigma-Aldrich). To induce FRB-FKBP heterodimerization of the split TEV⁴⁶, rapamycin (100 nM, Sigma) was added 10 h before cells were collected.

Immunoprecipitation and subcellular fractionation

Cells (1 × 10⁷) were lysed with a dounce homogenizer in 1 ml LP2 lysis buffer (20 mM Tris-HCl (pH 7.7), 100 mM NaCl, 10 mM NaF, 20 mM

Article

β -glycerophosphate, 5 mM MgCl₂, 0.1% Triton X-100, 5% glycerol), supplemented with benzonase (30 U/l; Santa Cruz) and complete protease inhibitor cocktail (Roche), and incubated on ice for 1 h. To preserve phosphorylations, lysis buffer was additionally supplemented with calyculin A (50 nM, LC-Laboratories) and microcystin LR (1 μ M, Alexis Biochemicals). If transmembrane proteins were to be analysed, the corresponding lysis reactions were cleared by low-speed centrifugation (2,500g for 10 min), giving rise to whole-cell extracts (WCE). In all other cases, lysis reactions were cleared by centrifugation at 16,000g for 30 min, resulting in lysates. For immunoprecipitations, 1 ml of WCE or lysate was rotated over 10 μ l of antibody-carrying beads for 4–12 h at 4 °C and washed 5× with lysis buffer. For Extended Data Figs. 4c and 8c, immobilized MCL1 or BCL-XL–BAK–BAD complexes were incubated with separase before boiling in SDS-sample buffer. For Fig. 4e, incubation also included NEK2A and ATP. For cleavage of MCL1-TEV in lysate (Fig. 2a), 20 U of His₆-TEV protease was added at 18 °C and immunoprecipitation was started 30 min thereafter. Intact mitochondria were enriched and separated from cytosol as described²⁷.

RNA interference

For efficient knockdown, cells were transfected with calcium phosphate or RNAiMax (Invitrogen) using 70–100 nM siRNA duplex directed against *PTTG1 (SECURIN)*: 5'-UCUUAGUGCUUCAGAGUUUGUGUUAU-3', *SGO2*: 5'-GAACACAUUCUUCGCCUATT-3', *ESPL1 (SEPARASE)*: 5'-AACUGUUCUACCUCCAAGGUUAGAUUU-3', *NEK2A*: 3'-UUCUGAG AGUCAGCUCACA-5', *MCL1*: 5'-CGAAGGAAGUAUCGAAUUTT-3', *BCL2L1 (BCL-XL)*: 5'-CCAGGGAGCUUGAAAGUUUTT-3', *SGO1*: 5'-GAUGACAGCUCCAGAAAUTT-3', *CDC45 (SORORIN)*: 3'-UGGAG GAGCUCGAGACGGA-5', *BUB1B (BUBR1)*: 5'-GGACACATTTAGATG CACTTT-3' and/or *MAD2*: 5'-GCTTGTAACTACTGATCTTT-3'. For transfer of siRNA into NIH/3T3 cells, we used Lipofectamine 2000 (Invitrogen) according to an optimized protocol supplied by the manufacturer. The following pre-designed siRNAs (IDT) were used: mm.RI.MCL1.13.1: 5'-GAGUGCUGACUAGAUGAUCAACAUUCAUCUAGUC-3', mm.RI.MCL1.13.2: 5'-GCGUAAACCAAGAAAGCUUCGAUGAAGCUUCUUGG-3' (a mixture of both was used for Fig. 4d), mm.RI.PTTG1.13.1 ('a' in Extended Data Fig. 2g): 5'-UAUCUUUGUUGUAAGGAUUCAUU AUCCUUUAAC-3', mm.RI.PTTG1.13.2 ('b' in Extended Data Fig. 2g): 5'-AUCACCGAGAAGUCUACUGUGUCUUAGUAGACUUCU-3', mm.RI.SGOL2a.13.1 ('a' in Extended Data Fig. 2g): 5'-ACCUCU UCAGUAUCAAGAAAGGUUGUCUUGAUACUG-3' and mm.RI.SGOL2a.13.2 ('b' in Extended Data Fig. 2g): 5'-GAAACUUAGAC AAAAGGUUCGAUUUACCUUUUGUCU-3'. Luciferase siRNA (GL2) served as control (Ctrl). If depletion of the corresponding protein caused DiM, siRNA transfection was performed during thymidine block and cells were collected upon entering mitosis. In all other cases transfection was performed on asynchronous cells 12 h before synchronization.

Fluorescence microscopy

To detect apoptosis in fixed samples, Hek293T cells were grown on poly-lysine-coated glass coverslips and processed 10–12 h after release from thymidine arrest. Different staining and fixation procedures were carried out. Where indicated, cells were stained with annexin V–FITC and propidium iodide according to the manufacturer's protocol (Annexin V–FITC Apoptosis Detection Kit, Abcam), washed once with corresponding binding buffer and mounted onto coverslips in 5 μ l DAPI-Fix (1× MMR, 48% glycerol, 11% formaldehyde, 1 mg/ml Hoechst 33342)⁴⁷. To label intact mitochondria, 200 nM MitoTracker (Orange CMTMRos, Invitrogen) was added 10 h after release from thymidine to Hek293T cells in serum-free cell culture medium and incubated for 45 min before cells were fixed. If additional antibody staining was performed, corresponding coverslips were washed once with PBS, fixed with fixation solution (PBS, 3.7% formaldehyde) for 15 min at room temperature, and then washed twice with quenching solution (PBS, 100 mM glycine). Cells were then treated with permeabilization solution

(PBS, 0.5% Triton X-100) for 5 min, washed with PBS and incubated in blocking solution (PBS, 1% (w/v) BSA) overnight at 4 °C. Coverslips were transferred into a wet chamber, incubated with primary antibodies for 1 h, washed four times with PBS-Tx (PBS, 0.1% Triton X-100), incubated with fluorescently labelled secondary antibodies for 1 h, washed once with PBS-Tx, stained for 10 min with 1 μ g/ml Hoechst 33342 in PBS-Tx, washed four times and mounted in 20 mM Tris-HCl (pH 8.0), 2.33% (w/v) 1,4-diazabicyclo(2.2.2)octane, 78% glycerol on a glass slide. Immunofluorescence microscopy of fixed cells was performed on a DMI 6000 inverted microscope (Leica) using a HCX PL APO 100 \times /1.40–0.70 oil objective. Z-stack series were collected in 0.2- μ m increments over 10 μ m, deconvoluted (blind algorithm) and, where indicated, projected into one plane using the LAS-AF software. For 2D SIM, cells were grown on Precision cover glasses (Marienfeld) and imaged with the Nikon Eclipse Ti2 using a SRAPO TIRF AC100 \times H objective. Z-stacks were captured in 0.1- μ m increments over 2 μ m, processed using the stack reconstruction mode and visualized by volume and maximum projection of the NIS-Elements AR software (Nikon). Chromosome spreads were prepared as described⁴⁸. For video microscopy, transfected HeLa-K or *X. laevis* S3 cells were released from single 20 h thymidine block (how long?), transferred into a μ -Slide 8-well (Ibidi) dish, and imaged starting 5–6 h later over a period of 5–15 h in 8–10-min intervals on a DMI 6000 inverted microscope (Leica) using a HCX PL APO 40 \times /0.85 CORR (HeLa) or HCX PL FLUOTAR L 20 \times /0.40 CORR PH1 (S3) objective and the corresponding LAS AF600 software. To visualize chromatin, SiR-Hoechst (200 nM)⁴⁹ and Verapamil (1 μ M, both from Spirochrome) were added to the culture medium 6 h before imaging. Where indicated, medium was additionally supplemented with IncuCyte Caspase 3/7 reagent (5 μ M, Essen Bioscience)⁵⁰.

In vitro kinase and cleavage assay

MCL1 from different origins served as substrates for in vitro phosphorylation reactions. Immunoprecipitated MCL1 bound to 10 μ l beads, 3 μ l of in vitro translated MCL1 Δ TM (TNT Quick-coupled Transcription and Translation kit, reticulocyte lysate-based, Promega) or 2 μ g bacterially expressed, purified MCL1 Δ TM were combined with 'cold' ATP (5 μ M) and 40 μ Ci γ -³³P-ATP (Hartmann Analytic) for radioactive labelling or only with cold ATP (1 mM) for non-radioactive phosphorylation. Reactions of 25 μ l were assembled in kinase buffer (10 mM Hepes-KOH (pH 7.7), 50 mM NaCl, 25 mM NaF, 1 mM EGTA, 20% glycerol, 10 mM MgCl₂, 10 mM DTT) including 1 μ l of NEK2A- Δ MR, NEK2B- Δ MR or Δ 86-cyclinA2-CDK1/2 (corresponding to 12.5 × 10⁵ transfected Hek293T cells each; see below), 0.4 μ g of His₆-tagged Δ 90-cyclinB1-CDK1⁵¹, 0.1 μ g of PLK1 (ProQinase, No. 0183-0000-1) or 0.1 μ g of GST-tagged Aurora B (PRECISIO-Kinase, A2108). To specifically inhibit phosphorylation, the following kinase inhibitors were used: RO-3306 (2 μ M, Santa-Cruz), BI-2536 (100 nM, Boehringer-Ingelheim), staurosporine (300 nM, Abcam) and ZM-447439 (0.5 μ M, Tocris). For reactions containing BCL-XL Δ TM, 3 μ l IVT served as substrate. To test kinase activity, 2 μ g each of histone H1 (NEB) or myelin basic protein (MBP, Upstate Biotechnology) were used. Kinase reactions were incubated for 30 min at 37 °C, subjected to SDS-PAGE, blotted onto PVDF membrane (SERVA) and analysed by autoradiography using a phospho-sensitive imaging plate (Fujifilm). The same membrane was re-activated with methanol and further analysed by immunoblotting. For cleavage assays, 12.5 μ l reactions were incubated with 1 μ l separase (active P1127A variant or protease-dead (PD) C2029S variant)^{39,41}, 1 U human caspase 3 (Enzo) or 20 U TEV protease, incubated for 30 min at room temperature (separase) or 37 °C (both others) and stopped by addition of SDS-sample buffer.

Recombinant protein expression and purification

To produce recombinant NEK2A- Δ MR (active or kinase-dead (KD, L37M), NEK2B- Δ MR and Δ 86-cyclinA2 (in complex with endogenous CDK1/2), 10 × 10⁷ Hek293T cells were transfected with the corresponding plasmids to express the kinases in fusion with a GFP-SUMOstar tag⁵²,

supplemented with taxol 24–48 h thereafter and collected 12 h later. Lysates in LP2 (including protease and phosphatase inhibitors) were cleared by centrifugation for 30 min at 16,500g and rotated for 4 h at 4 °C with anti-GFP nanobody beads (0.1 ml corresponding to 1 mg nanobody). Immobilized kinases were washed three times in LP2 (200 g, 1 min, 4 °C), transferred into cleavage buffer (10 mM Hepes-KOH (pH 7.7), 50 mM NaCl, 25 mM NaF, 1 mM EGTA, 20% glycerol) and incubated with 40 µg His₆-SUMOstar protease⁵² for 45 min at 18 °C. Eluates (80 µl) were snap-frozen and stored in aliquots at –80 °C. His₆-SUMO1–MCL1ΔTM was expressed from a pET28-derivative in *Escherichia coli*. Rosetta 2 DE3 (Novagen). Bacteria were lysed in LP1 (PBS, 5 mM imidazole, 0.5 mM DTT and an additional 400 mM NaCl) and purified over Ni²⁺-NTA-agarose (Qiagen) according to standard procedures. The eluate in PBS supplemented with 250 mM imidazole, 0.5 mM DTT and an additional 400 mM NaCl (pH adjusted to 7.5 with HCl) was dialysed against LP1 for 12 h at 4 °C in the presence of 10 ng His₆-Senp2⁵³ per 100 µg MCL1 and then rotated for 3 h over 9/10th the amount of fresh Ni²⁺-NTA-agarose. The flow-through containing pure MCL1ΔTM was dialysed against PBS and stored in aliquots at –80 °C.

Flow cytometry

To measure apoptosis *in vivo*, HeLa-K cells transfected with corresponding siRNAs and plasmids were collected by gentle trypsinization, washed once with medium, and then stained with annexin V-FITC and propidium iodide according to the manufacturer's protocol (Abcam, ab14085). Samples were analysed immediately on a Cytomix FC 500 (Beckman Coulter) using an FL1 signal detector for FITC and FL2 for propidium iodide and counting at least 20,000 single cells per condition. Flow cytometry of propidium iodide-stained cells was done as described⁴².

Statistics and reproducibility

No statistical methods were used to predetermine sample size. Experiments analysed by immunoblotting or autoradiography were repeated 2–4 times with similar results (2–4 biological replicates). For quantitative analyses of chromosome spreads, clonogenic assays, and IFM specimen, the investigators were blinded to sample allocation. Otherwise, experiments were not randomized.

Reporting summary

Further information on research design is available in the Nature Research Reporting Summary linked to this paper.

Data availability

The data that support the findings of this study are available within the paper. Source Data for Figs. 1–4 and Extended Data Figs. 1–12 are provided with the paper. Data or other materials are available from the corresponding author upon reasonable request.

39. Stemmann, O., Zou, H., Gerber, S. A., Gygi, S. P. & Kirschner, M. W. Dual inhibition of sister chromatid separation at metaphase. *Cell* **107**, 715–726 (2001).
40. Wolf, P. G., Cuba Ramos, A., Kenzel, J., Neumann, B. & Stemmann, O. Studying meiotic cohesin in somatic cells reveals that RecQL-containing cohesin requires Stag3 to function and is regulated by Wapl and sororin. *J. Cell Sci.* **131**, jcs212100 (2018).
41. Hellmuth, S. et al. Human chromosome segregation involves multi-layered regulation of separase by the peptidyl-prolyl-isomerase Pin1. *Mol. Cell* **58**, 495–506 (2015).
42. Hellmuth, S., Böttger, F., Pan, C., Mann, M. & Stemmann, O. PP2A delays APC/C-dependent degradation of separase-associated but not free securin. *EMBO J.* **33**, 1134–1147 (2014).
43. Hellmuth, S., Gutiérrez-Caballero, C., Llano, E., Pendás, A. M. & Stemmann, O. Local activation of mammalian separase in interphase promotes double-strand break repair and prevents oncogenic transformation. *EMBO J.* **37**, e99184 (2018).
44. To, T. L. et al. Rational design of a GFP-based fluorogenic caspase reporter for imaging apoptosis *in vivo*. *Cell Chem. Biol.* **23**, 875–882 (2016).
45. Agudelo, D. et al. Marker-free coselection for CRISPR-driven genome editing in human cells. *Nat. Methods* **14**, 615–620 (2017).
46. Wehr, M. C. et al. Monitoring regulated protein–protein interactions using split TEV. *Nat. Methods* **3**, 985–993 (2006).
47. Murray, A. W. Cell cycle extracts. *Methods Cell Biol.* **36**, 581–605 (1991).
48. McGuinness, B. E., Hirota, T., Kudo, N. R., Peters, J. M. & Nasmyth, K. Shugoshin prevents dissociation of cohesin from centromeres during mitosis in vertebrate cells. *PLoS Biol.* **3**, e86 (2005).
49. Lukinavičius, G. et al. SiR-Hoechst is a far-red DNA stain for live-cell nanoscopy. *Nat. Commun.* **6**, 8497 (2015).
50. Hanson, K. M. & Finkelstein, J. N. An accessible and high-throughput strategy of continuously monitoring apoptosis by fluorescent detection of caspase activation. *Anal. Biochem.* **564–565**, 96–101 (2019).
51. Gorr, I. H., Boos, D. & Stemmann, O. Mutual inhibition of separase and Cdk1 by two-step complex formation. *Mol. Cell* **19**, 135–141 (2005).
52. Liu, L., Spurrier, J., Butt, T. R. & Strickler, J. E. Enhanced protein expression in the baculovirus/insect cell system using engineered SUMO fusions. *Protein Expr. Purif.* **62**, 21–28 (2008).
53. Butt, T. R., Edavettal, S. C., Hall, J. P. & Mattern, M. R. SUMO fusion technology for difficult-to-express proteins. *Protein Expr. Purif.* **43**, 1–9 (2005).
54. Hames, R. S. & Fry, A. M. Alternative splice variants of the human centrosome kinase Nek2 exhibit distinct patterns of expression in mitosis. *Biochem. J.* **361**, 77–85 (2002).
55. Inoshita, S. et al. Phosphorylation and inactivation of myeloid cell leukemia 1 by JNK in response to oxidative stress. *J. Biol. Chem.* **277**, 43730–43734 (2002).
56. Maurer, U., Charvet, C., Wagman, A. S., Dejardin, E. & Green, D. R. Glycogen synthase kinase-3 regulates mitochondrial outer membrane permeabilization and apoptosis by destabilization of MCL-1. *Mol. Cell* **21**, 749–760 (2006).

Acknowledgements We thank T. U. Mayer for suggesting the concept of the DMC, R. Youle and M. Orth for cell lines, D. Pfeiffer for help with the 2D SIM, S. Heidmann, T. Klecker, and P. Wolf for critical reading of the manuscript, and J. Hübner and M. Hermann for technical assistance. This work was supported by a grant (STE997/4-2) from the Deutsche Forschungsgemeinschaft (DFG) to O.S.

Author contributions S.H. carried out all experiments. S.H. and O.S. co-designed the research and wrote the paper.

Competing interests The authors declare no competing interests.

Additional information

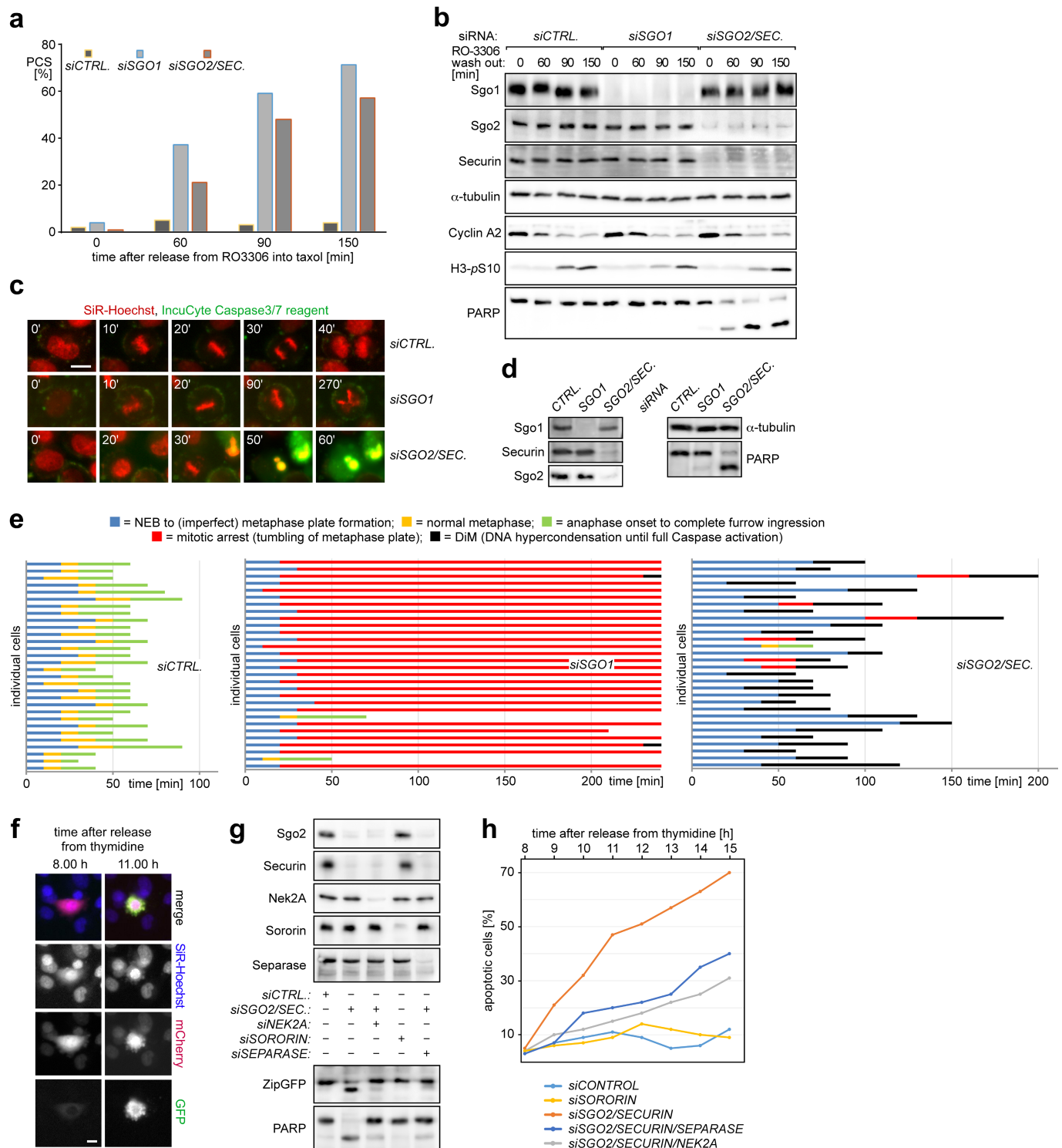
Supplementary information is available for this paper at <https://doi.org/10.1038/s41586-020-2187-y>.

Correspondence and requests for materials should be addressed to O.S.

Peer review information *Nature* thanks Andreas Villunger, Hongtao Yu and the other, anonymous, reviewer(s) for their contribution to the peer review of this work.

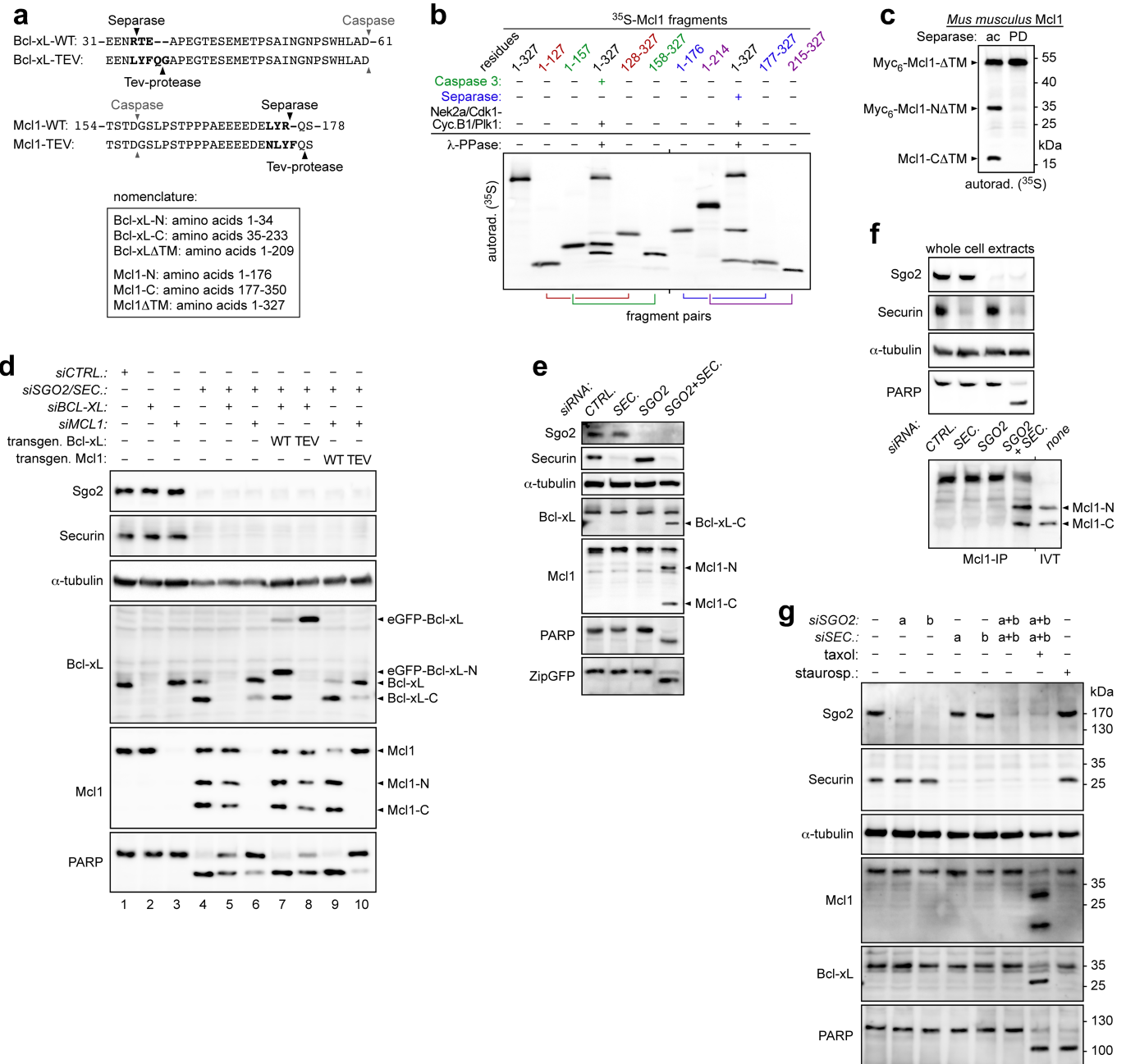
Reprints and permissions information is available at <http://www.nature.com/reprints>.

Article



Extended Data Fig. 1 | Premature activation of separase rather than loss of cohesion triggers DiM. **a**, Premature sister chromatid separation (PCS) was quantified by chromosome spreading from siRNA-transfected HeLa-K cells at different times after release from RO-3306/G2 arrest. **b**, Immunoblots of cells from **a**. **c–e**, HeLa-K cells transfected with the indicated siRNAs and cultured in the presence of SiR-Hoechst⁴⁹ and a fluorogenic caspase 3/7 reporter⁵⁰ were analysed by video fluorescence microscopy. Shown are representative stills (**f**), immunoblots (**g**), and line graphs (**h**) of the percentages of GFP-positive (apoptotic) cells. The ZipGFP plasmid also expresses mCherry as a control. Scale bar, 10 μ m.

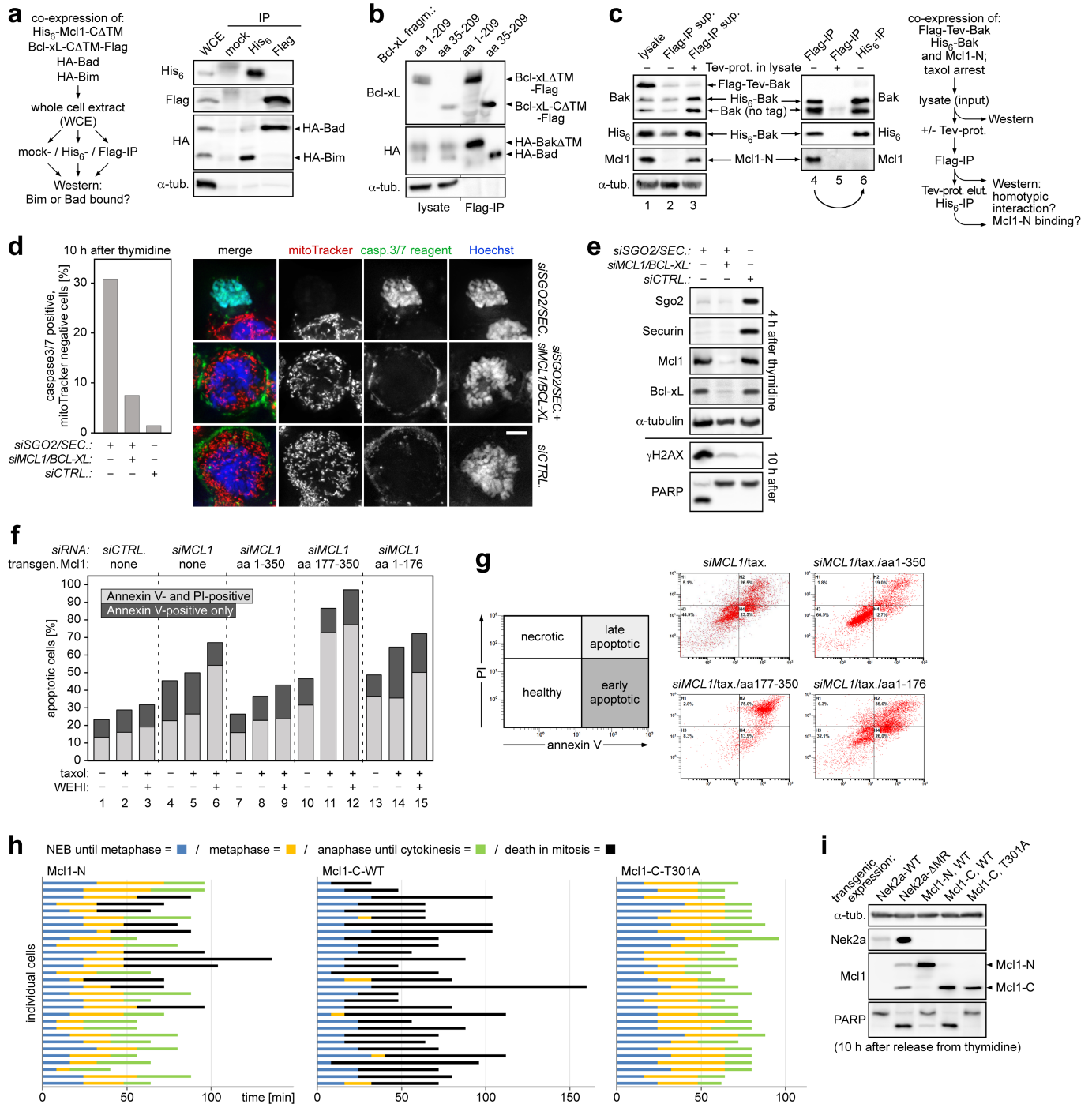
(**c**; scale bar, 10 μ m), immunoblots (**d**), and cell fate profiles (**e**). **f–h**, HeLa-K cells expressing the caspase 3 reporter ZipGFP⁴⁴ were transfected with the indicated siRNAs, supplemented with SiR-Hoechst and followed by video microscopy. At least 100 cells were counted per time point and condition. Shown are representative stills (**f**), immunoblots (**g**), and line graphs (**h**) of the percentages of GFP-positive (apoptotic) cells. The ZipGFP plasmid also expresses mCherry as a control. Scale bar, 10 μ m.



Extended Data Fig. 2 | Characterization of MCL1 (and BCL-XL) cleavage by separase (and caspase 3). **a**, Sequence stretches of wild-type BCL-XL and MCL1 and TEV variants thereof. Differing amino acids are in bold. Arrowheads show protease cleavage sites. **b**, Separase and caspase 3 cleave MCL1 after Arg176 and Asp157, respectively, as mapped by in vitro-expressed fragments. **c**, Separase cleaves MCL1 after 154-DXXR-157. Autoradiograph of in vitro-translated, NEK2A/separase-treated mouse ³⁵S-MCL1. PD, protease-dead (C2029S); Ac, active (P1127A); ΔTM, transmembrane domain deleted. **d**, Immunoblots of

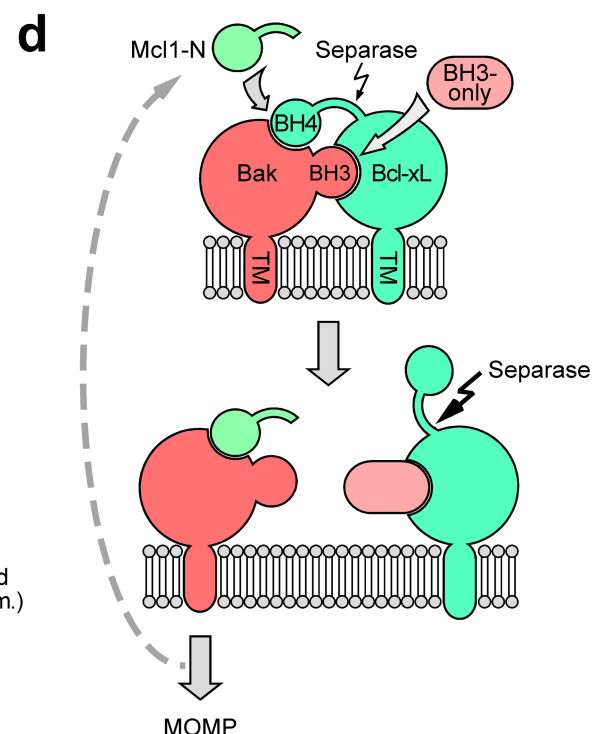
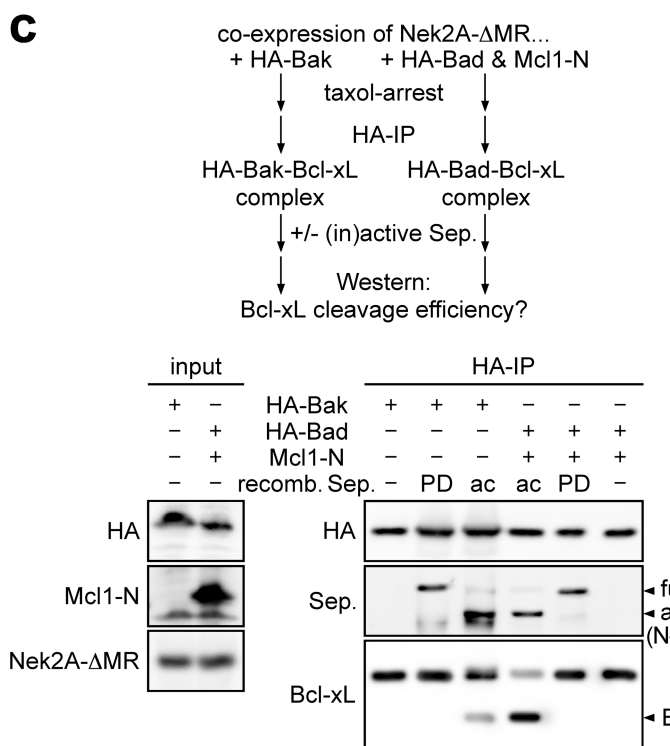
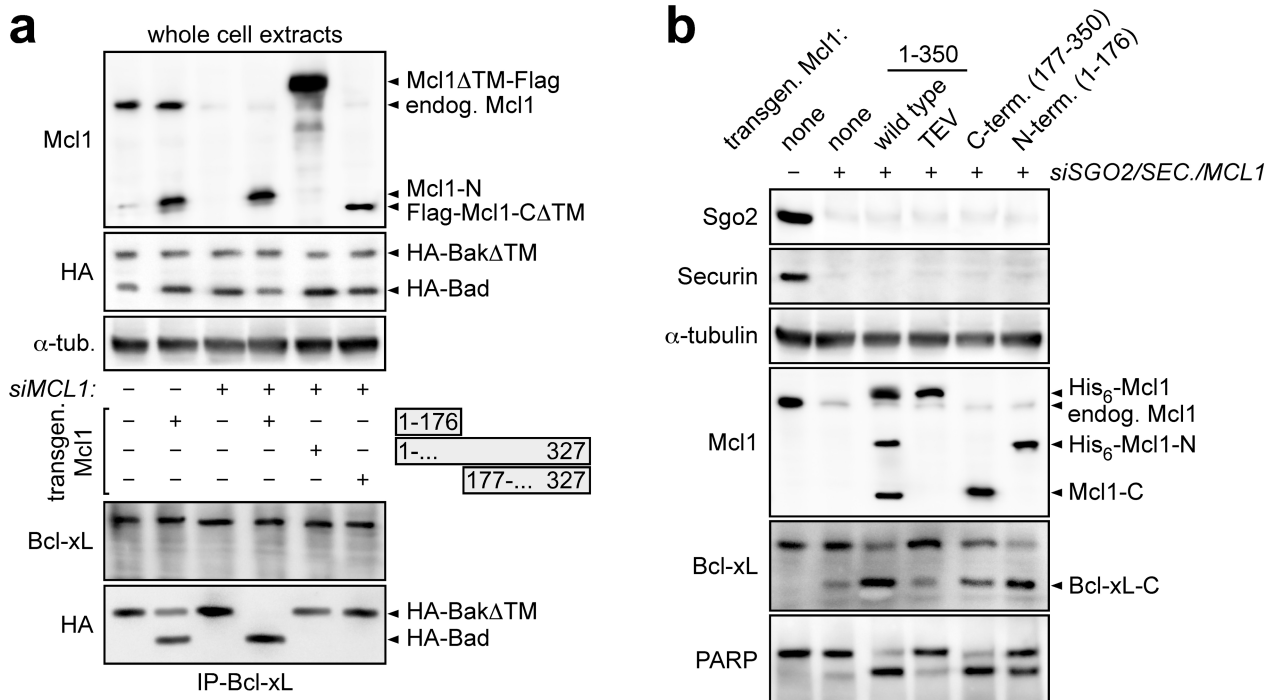
taxol-arrested Hek293T cells transfected with siRNAs and expression plasmids as indicated. During separase-triggered DiM, MCL1 cleavage stimulates BCL-XL cleavage and vice versa, which—at least in the case of MCL1—is mediated by the corresponding N-terminal fragment (Extended Data Fig. 4b). **e**, Co-depletion of SGO2 and securin induces cleavage of MCL1 and BCL-XL followed by apoptosis in non-transformed cells. Immunoblots of siRNA-transfected, taxol-arrested hTERT RPE1 cells expressing ZipGFP. **f**, MCL1 is cleaved after R176 during DiM of SGO2- and securin-depleted cells. Immunoblots of extracts and MCL1 immunoprecipitates (IP) from taxol-arrested Hek293T cells transfected with the indicated siRNAs. IVT, in vitro translated. **g**, Mouse MCL1 and BCL-XL are cleaved and DiM is triggered upon separase deregulation in mouse cells. NIH/3T3s cells transfected with siRNAs and treated with taxol and staurosporine as indicated were analysed by immunoblotting.

Article



Extended Data Fig. 3 | Characterization of separase cleavage fragments of MCL1 and BCL-XL. **a**, The C-terminal separase cleavage fragments of MCL1 and BCL-XL preferentially bind BIM and BAD, respectively. Experimental setup and immunoblots of the indicated immunoprecipitation from taxol-arrested Hek293T cells co-expressing His₆-MCL1-CΔTM, BCL-XL-CΔTM-Flag, HA-BAD, and HA-BIM. **b**, BCL-XL and BCL-XL-C bind BAK and BAD, respectively. Immunoblots of Flag immunoprecipitation from transfected, mitotic Hek293T cells expressing the indicated Flag-tagged BCL-XL fragments together with HA-tagged BAK and BAD. **c**, MCL1-N interacts with BAK. Experimental setup and immunoblots of lysate and consecutive Flag and His₆ immunoprecipitations from transfected, mitotic Hek293T cells co-expressing Flag-TEV-BAK, His₆-BAK, and MCL1-N. TEV protease supplementation of lysate served as a negative control. Self-interaction of BAK is mutually exclusive with binding of MCL1-N. **d**, Separase-induced DiM is suppressed by knock-down of

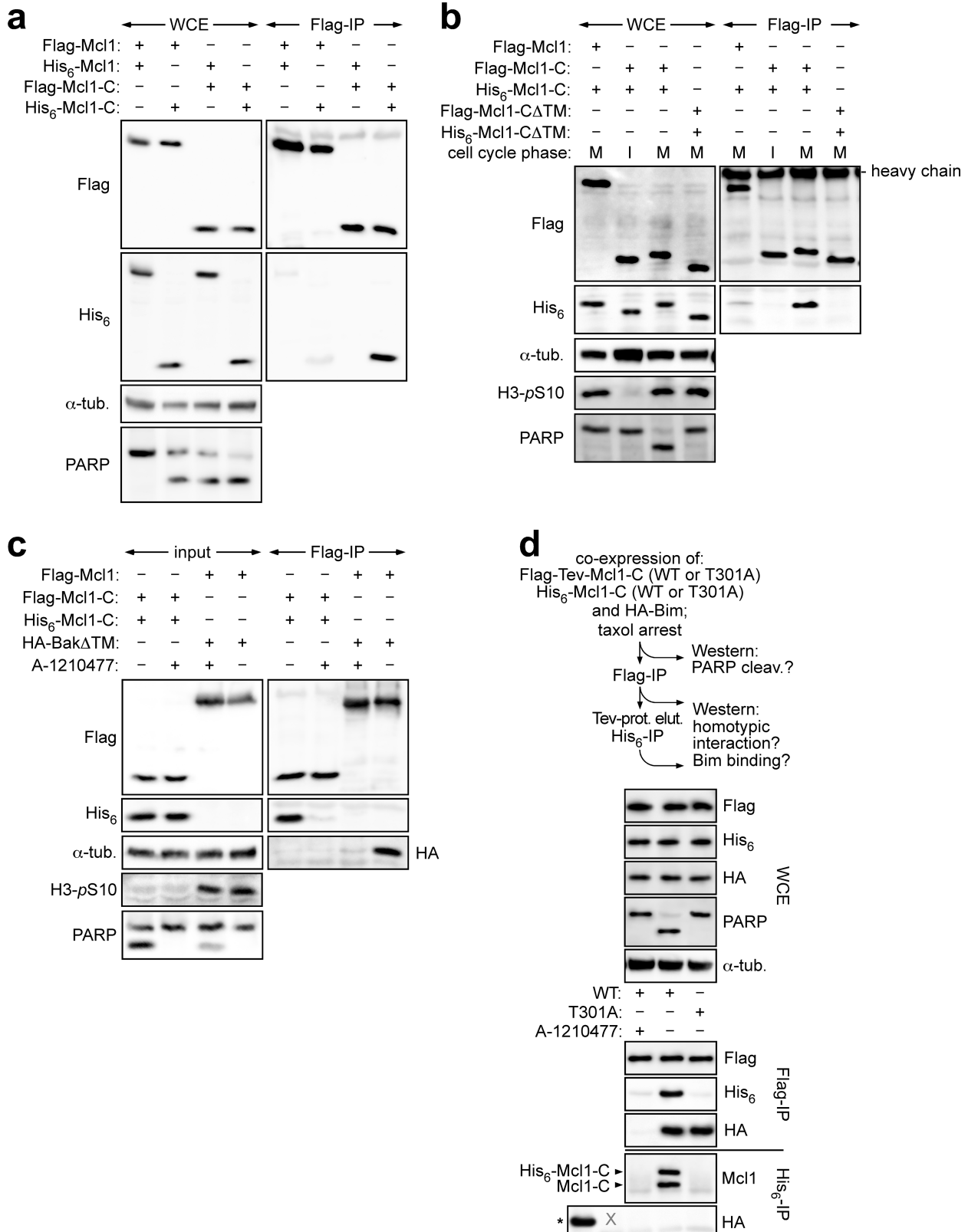
MCL1 and BCL-XL. Quantification and representative images of siRNA-transfected, mitotic Hek293T cells cultivated in the presence of mitoTracker and a fluorogenic caspase 3/7 reporter before fixation and Hoechst staining. At least 100 cells each were counted. Scale bar, 5 μm. **e**, Immunoblots of cells from **d**, MCL1-N and -C promote DiM. Plot of early (dark grey) and late (light grey) apoptosis as judged by flow cytometric analysis of propidium iodide and annexin V staining of Hek293T cells transfected with siRNAs and expression vectors for transgenic MCL1 (fragments) and supplemented with taxol and BCL-XL inhibitor WEHI-539 (WEHI) as indicated. **g**, Representative 2D scatter plots of cells from **f** and their interpretation. **h**, Induction of DiM by MCL1-C does not require taxol treatment but does require Thr301. Cell fate profiles of HeLa-K cells expressing the indicated MCL1 fragments and cultured in the presence of SiR-Hoechst and a fluorogenic caspase 3/7 reporter. **i**, Immunoblot of cells from **h** and Extended Data Fig. 10a.



Extended Data Fig. 4 | MCL1-N enables BAD to replace BAK as an interactor of BCL-XL and enhances cleavage of BCL-XL by separase. a, MCL1-N causes a switch in the binding partner of BCL-XL from BAK to BAD. Immunoblots of BCL-XL immunoprecipitation from MCL1-depleted or control-treated, mitotic Hek293T cells co-expressing HA-BAK, HA-BAD and, where indicated, various MCL1 fragments. Separase was not deregulated in this experiment, which is why BCL-XL is not cleaved. **b,** Separase-dependent BCL-XL cleavage in cells is primarily stimulated by MCL1-N. Immunoblots of SGO2/securin/MCL1 triple-depleted or control-treated, prometaphase Hek293T cells expressing the indicated transgenic MCL1 variants. **c,** Separase prefers BCL-XL in complex with BAD as a substrate rather than BAK. Experimental setup and immunoblots

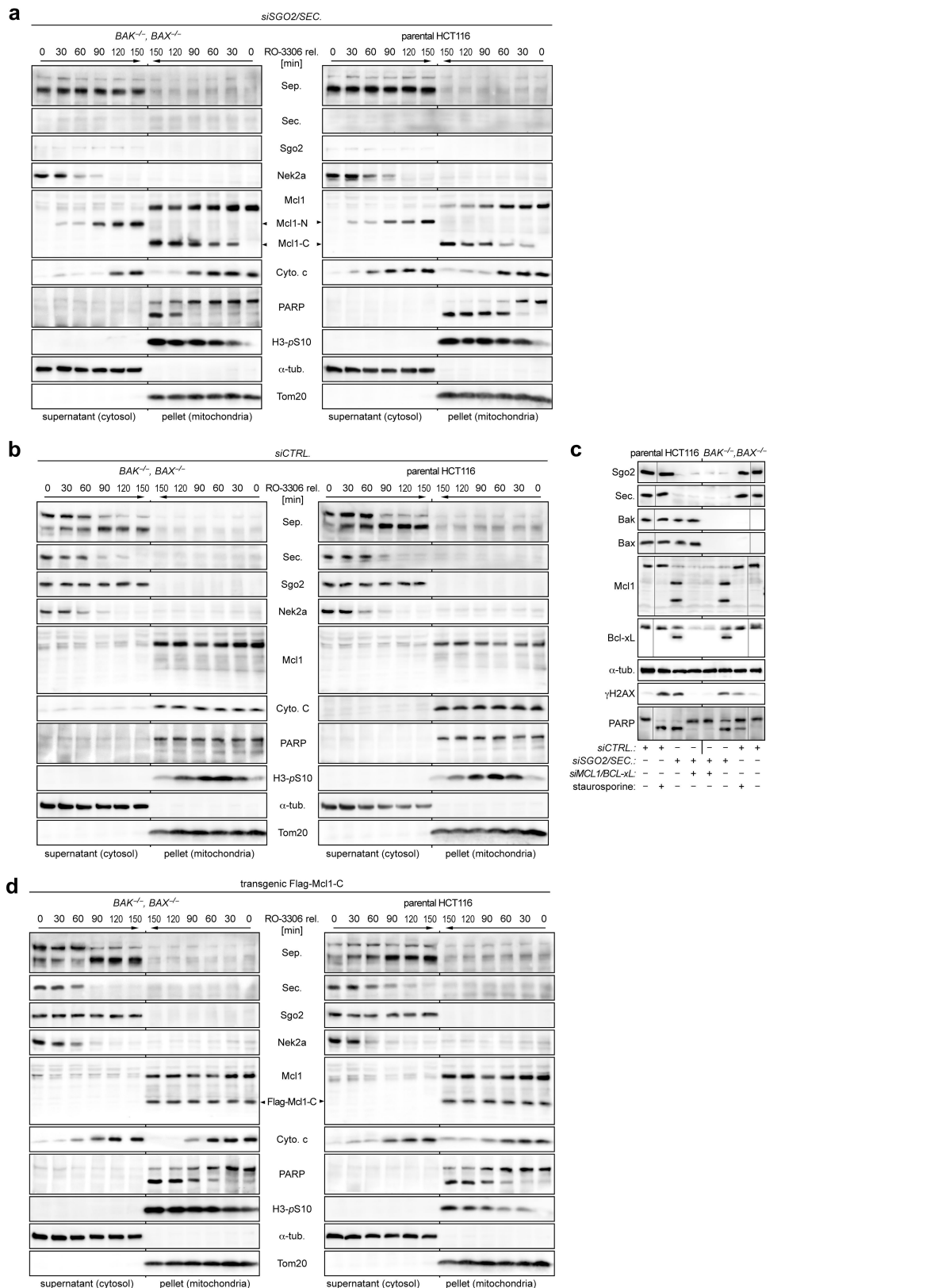
of HA immunoprecipitation from taxol-arrested Hek293T cells expressing NEK2A-ΔMR and either HA-BAK or HA-BAD plus MCL1-N. Before SDS-PAGE, samples were incubated with inactive (PD) or active (ac) separase or control treated (-). **d,** MCL1-N promotes apoptosis by a positive feedback mechanism. MCL1-N competitively displaces the BH4 domain of BCL-XL from BAK. Similar to cleavage by separase, this breaks the cooperative binding of BCL-XL to BAK, resulting in BH3-only proteins, such as BAD, excluding BAK from BCL-XL. At the same time, this renders BCL-XL a better separase substrate. MCL1-N acts catalytically, being released from BAK upon self-interaction and pore formation by the latter (dotted arrow; Extended Data Fig. 3c).

Article



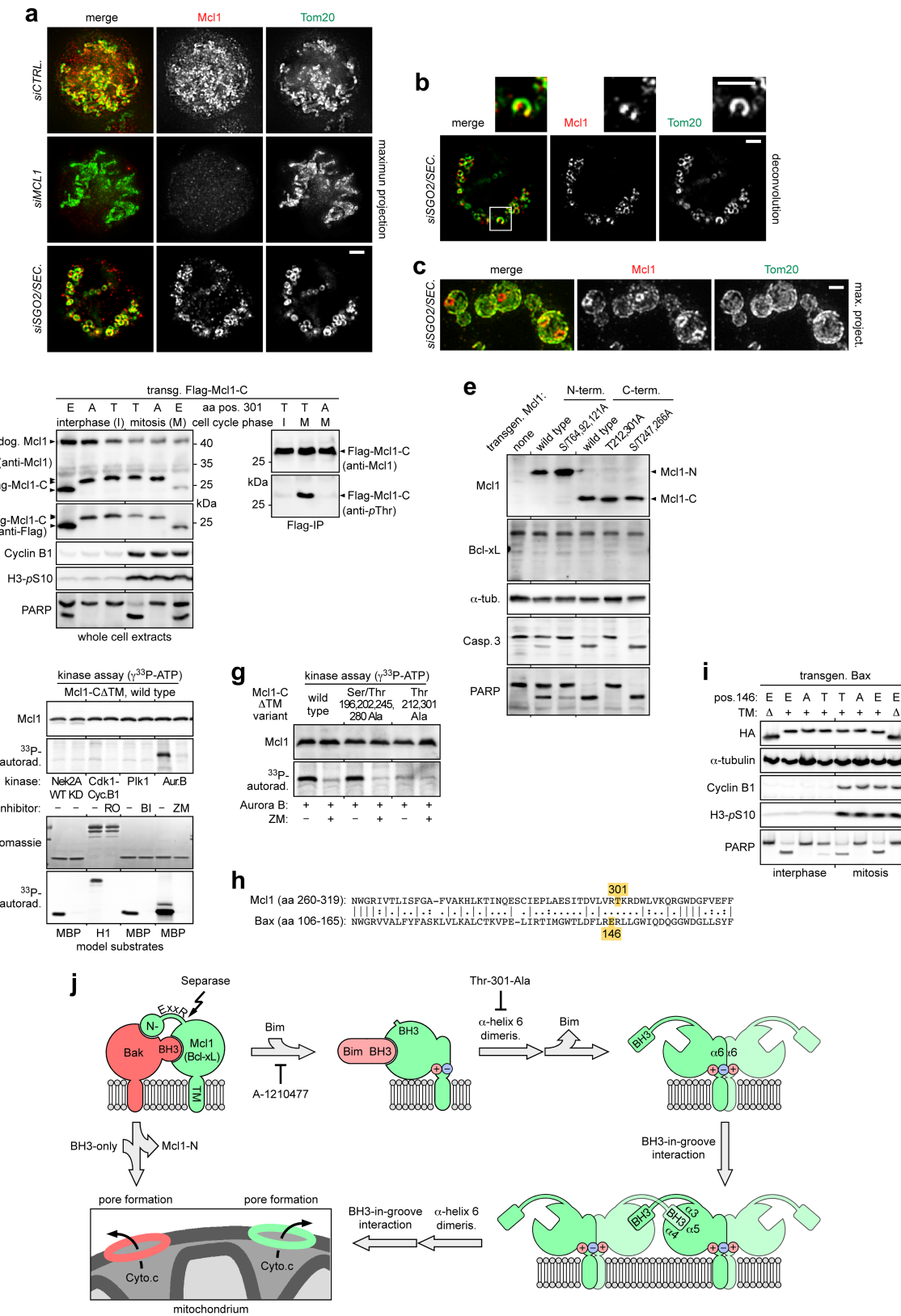
Extended Data Fig. 5 | Self-interaction of pro-apoptotic MCL1-C shares characteristics with pore formation by BAK/BAX but requires mitosis-specific phosphorylation. **a–c**, MCL1-C exhibits mitosis-specific self-interaction, which requires the transmembrane domain and an accessible BH3-binding groove. Immunoblots of Flag immunoprecipitation from mitotic or interphase HeK293T cells expressing MCL1 variants and supplemented with the MCL1 inhibitor A-1210477 as indicated. Blockade of the MCL1-BAK interaction served as a control for the effectiveness of A-1210477. **d**, The

homotypic interaction of MCL1-C is mutually exclusive with BIM binding. Top, experimental setup; bottom, immunoblots of consecutive Flag and His₆-immunoprecipitations from HeK293T cells expressing HA-BIM together with Flag-TEV and His₆-tagged forms of either wild-type MCL1-C or the T301A variant. X, irrelevant lane between HA-BIM control (asterisk) and His₆-immunoprecipitation samples. The T301A mutation prevents self-interaction of MCL1-C but not its association with BIM.



Extended Data Fig. 6 | BAK/BAX-independent release of cytochrome c by separate deregulation or MCL1-expression. **a, b,** Time-resolved immunoblots of cytosol and mitochondria-containing fractions from SGO2/securin-depleted or mock-transfected BAK^{-/-}, BAX^{-/-} and parental HCT116 cells released from a G2-arrest at t = 0 min. **c,** Immunoblots of taxol-arrested BAK^{-/-}, BAX^{-/-} and parental HCT116 cells that were transfected with siRNA and supplemented with staurosporine as indicated. Note the absence of MCL1 and

BCL-XL cleavage during staurosporine-induced apoptosis and suppression of siSGO2/siPTTG1-induced DiM by co-depletion of MCL1 and BCL-XL. Grey lines within panels are between lanes that were not directly juxtaposed but nevertheless originated from the same gel. **d,** Time-resolved immunoblots of cytosol and mitochondria-containing fractions from Flag-MCL1-C-expressing BAK^{-/-}, BAX^{-/-} and parental HCT116 cells released from G2-arrest at t = 0 min.

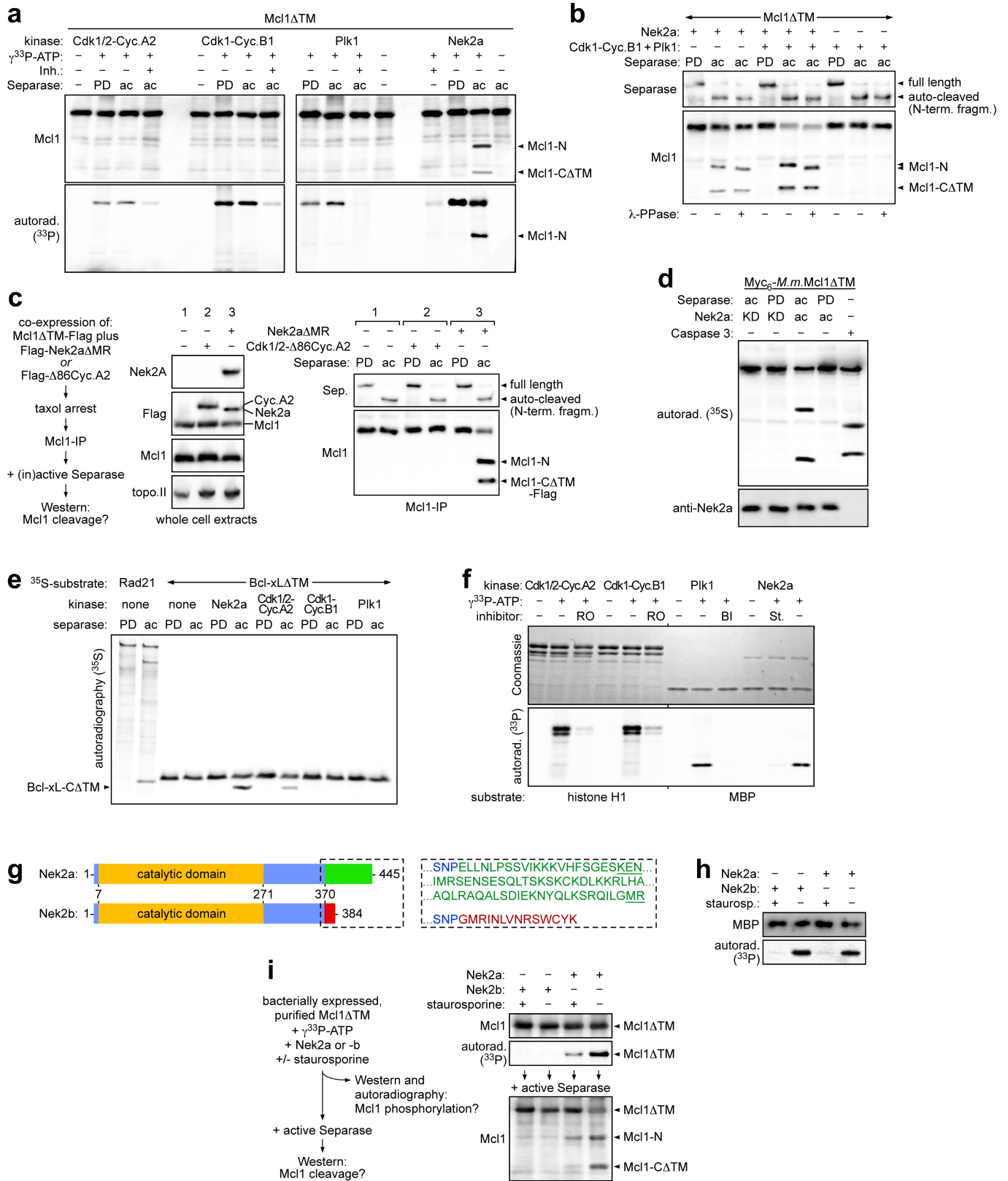


Extended Data Fig. 7 | See next page for caption.

Extended Data Fig. 7 | The pro-apoptotic effect of MCL1-C and BAX requires a negative charge at the end of α -helix 6. **a, b**, Immunofluorescence micrographs of taxol-arrested Hek293T cells transfected with the indicated siRNAs. Shown are maximum projections of 20 z-stacks (**a**) or a single, deconvoluted plane (**b**). The interruption of TOM20 rings by MCL1 dots is consistent with a cross-section through a fragmented mitochondrion containing an MCL1 ring. Scale bars, 3 μ m. **c**, MCL1-C is likely to form macropores into the mitochondrial outer membrane. Immunofluorescence 2D SIM of SGO2/securin-depleted Hek293T cells undergoing DiM. Note the absence of the mitochondrial outer membrane marker TOM20 from the centres of MCL1 rings. Scale bar, 0.5 μ m. **d**, Immunoblots of extracts and Flag immunoprecipitations from interphase or mitotic Hek293T cells expressing Flag-tagged MCL1-C-WT (T), MCL1-C(T301A) (A), or MCL1-C(T301E) (E). **e**, Identifying serine and threonine residues that affect the pro-apoptotic nature of MCL1-N and MCL1-C. Immunoblot of MCL1-depleted, taxol-arrested Hek293T cells expressing the indicated siRNA-resistant variants of MCL1-N or MCL1-C. BCL-XL is not cleaved during apoptosis if separase remains inhibited.

f, g, Aurora B kinase phosphorylates MCL1-C in vitro, probably at position 301 primarily. Immunoblots and autoradiographs of in vitro-translated wild-type MCL1-CATM and variants thereof after incubation with the indicated kinases and inhibitors in the presence of γ^{32} P-ATP. Activity of the recombinant kinase was confirmed using model substrates (**f**, lower panels). KD, kinase-dead; RO, RO-3306; BI, BI-2536; ZM, ZM-447439; MBP, myelin basic protein; H1, histone H1. **h**, Local alignment of MCL1 and BAX. Vertical lines and colons mark identical and chemically similar residues, respectively; dashes represent gaps. **i**, Immunoblots of interphase or mitotic Hek293T cells expressing BAX with (+) or without (Δ) TM and with Glu (E), Ala (A), or Thr (T) at position 146. **j**, Model of MOMP by MCL1-C homo-oligomerization. The indicated conformational changes are inspired by knowledge about BAK/BAX pore formation and their hierarchy was chosen to best explain our data; that is, why the T301A mutation abolished self-interaction of MCL1-C but left BIM binding unaffected (Extended Data Fig. 5d). Minus signs represent phosphorylated Thr301 and plus signs represent a nearby basic residue.

Article



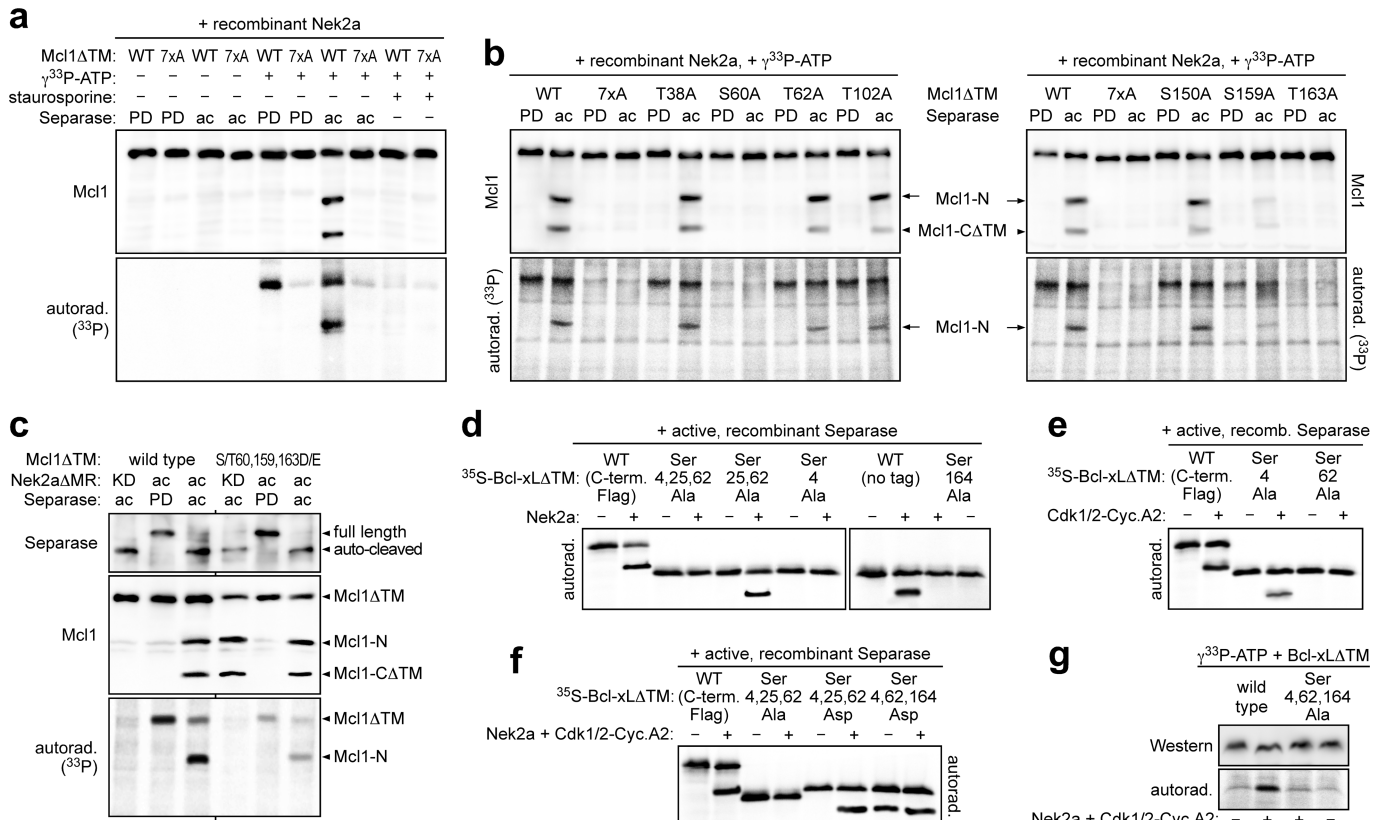
Extended Data Fig. 8 | See next page for caption.

Extended Data Fig. 8 | NEK2A kinase turns MCL1 and BCL-XL into separase substrates.

a, Autoradiographs and immunoblots of combined kinase (³³P-labelling) and cleavage (fragment-generation) assays using bacterially expressed, purified MCL1 Δ TM and kinases, specific inhibitors and active (ac) or inactive (PD) separase, as indicated. **b**, CDK1–cyclin B1 and PLK1 enhance separase-dependent cleavage of NEK2A-phosphorylated MCL1. Immunoblots of cleavage assays using bacterially expressed, purified MCL1 Δ TM and the indicated combination of kinases and separase variants. **c**, When immunoprecipitated from NEK2A- Δ MR-expressing, SAC-arrested cells, endogenous MCL1 is efficiently cleaved by separase in vitro. Left, experimental setup; right, immunoblots of cleavage assay combining active or inactive separase with MCL1 immunoprecipitation from prometaphase Hek293T cells expressing MCL1 Δ TM-Flag and, where indicated, Flag-NEK2A- Δ MR or N-terminally truncated (Δ 86) Flag–cyclin A2. **d**, Cleavage of mouse (*M.m*) MCL1 by separase also requires NEK2A-dependent phosphorylation. In vitro-translated ³⁵S-MYC6-*M.m*.MCL1 Δ TM was incubated with separase,

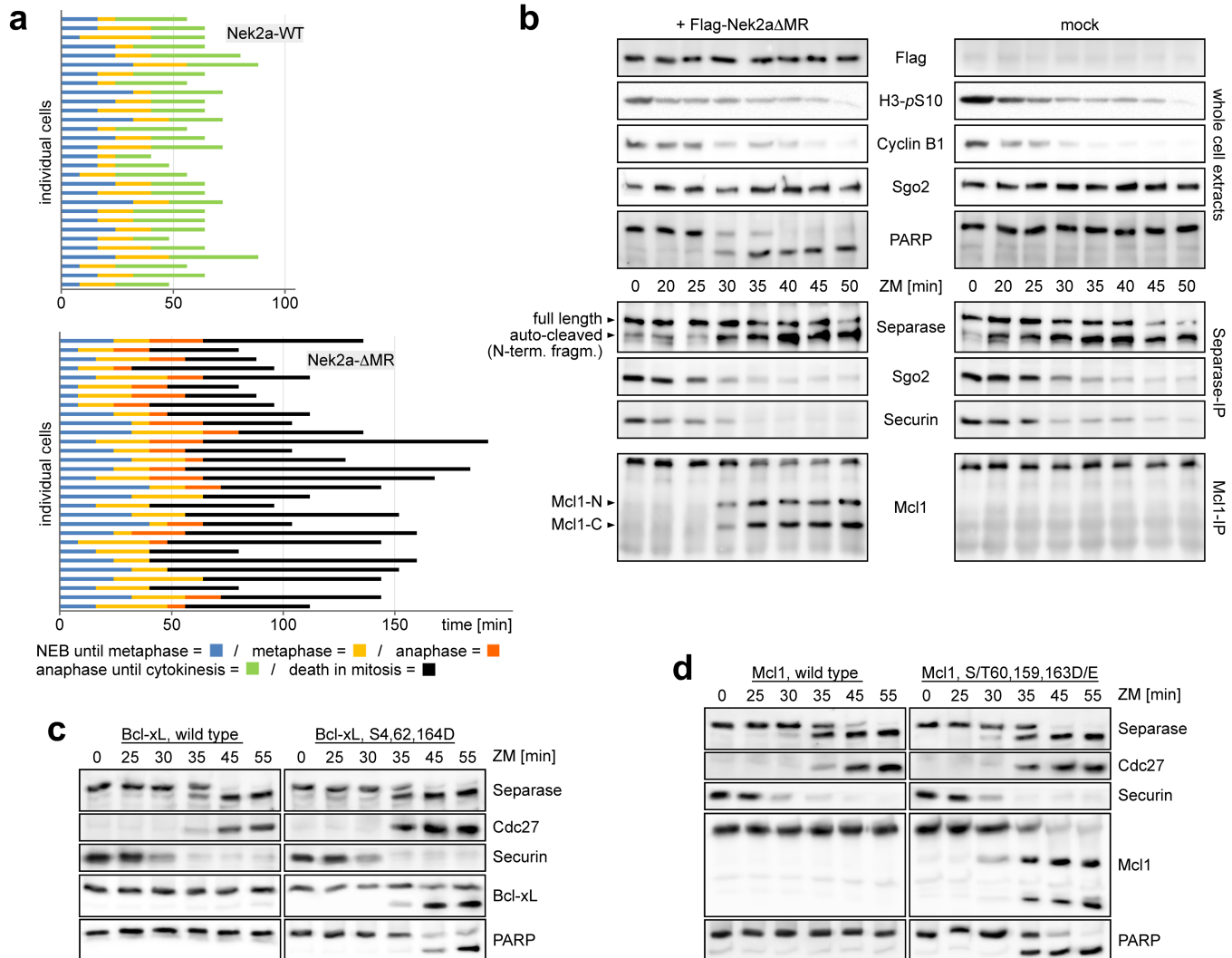
caspase 3 and NEK2A/ATP as indicated. Reactions were resolved by SDS-PAGE and analysed by autoradiography and immunoblotting. KD, kinase-dead (K37M). **e**, NEK2A and (to a lesser extent) CDK1/2–cyclin A2 sensitize BCL-XL to separase. Autoradiography of cleavage assay combining in vitro-translated ³⁵S-RAD21 (positive control) or ³⁵S-BCL-XL Δ TM with kinases/ATP and separase variants as indicated. **f**, Autoradiography of kinase assays (³³P-labelling) using model substrates and the kinases from **d**. **g–i**, The NEK2A-related NEK2B does not support separase-dependent MCL1 cleavage. **g**, Schematics and C-terminal sequences (dashed box) of NEK2A and NEK2B, which arise by alternative splicing of the same gene⁵⁴. NEK2A-specific, C-terminal degrons (KEN box and MR-tail) are underlined. **h**, Both NEK2A and NEK2B can phosphorylate the model substrate MBP. **i**, NEK2B cannot phosphorylate MCL1. Left, experimental setup; top right, kinase assay; bottom right, cleavage assay combining MCL1 Δ TM with NEK2A, NEK2B, staurosporine (kinase inhibitor) and active separase as indicated.

Article



Extended Data Fig. 9 | Mapping cleavage-relevant phosphorylation sites within MCL1 and BCL-XL. **a, b**, Cleavage of MCL1 by separase essentially requires NEK2A-dependent phosphorylation of Ser60 and Thr163. Autoradiographs and immunoblots of combined kinase (^{33}P -labelling) and cleavage (fragment-generation) assays. Prior to analysis, in vitro-translated, wild-type MCL1ΔTM and variants thereof were incubated with active NEK2A, $\gamma^{33}\text{P}$ -ATP, staurosporine, and active (ac) or inactive (PD) separase as indicated. In vivo phosphorylation of Ser159 and Thr163 has previously been reported^{55,56}. In vivo phosphorylation of Ser60 was detected by a phosphorylation-specific antibody (Fig. 4c, Extended Data Fig. 11d, e). **c**, Separase-dependent cleavage of MCL1(S/T60,159,163D/E) is independent of NEK2A. Immunoblots and

autoradiography of combined kinase (^{33}P) and cleavage assay. **d–f**, In vitro-translated, ^{35}S -labelled wild-type BCL-XLΔTM and variants thereof were incubated with the indicated kinases (+) or reference buffers (-) and active separase before SDS-PAGE and autoradiography. **d**, NEK2A-stimulated cleavage of BCL-XL by separase essentially requires Ser4 and Ser164. **e**, CDK1/2-cyclin A2-stimulated cleavage of BCL-XL by separase essentially requires Ser62. In vivo phosphorylation of Ser62 has been previously reported⁴⁸. **f**, Separase-dependent cleavage of BCL-XL(S4,62,164D) occurs independently of NEK2A and CDK1/2-cyclin A2. **g**, Autoradiograph and immunoblot of kinase assay using in vitro-translated, wild-type BCL-XLΔTM or its S4,62,164A variant and $\gamma^{33}\text{P}$ -ATP in combination with the indicated kinases (+) or reference buffers (-).

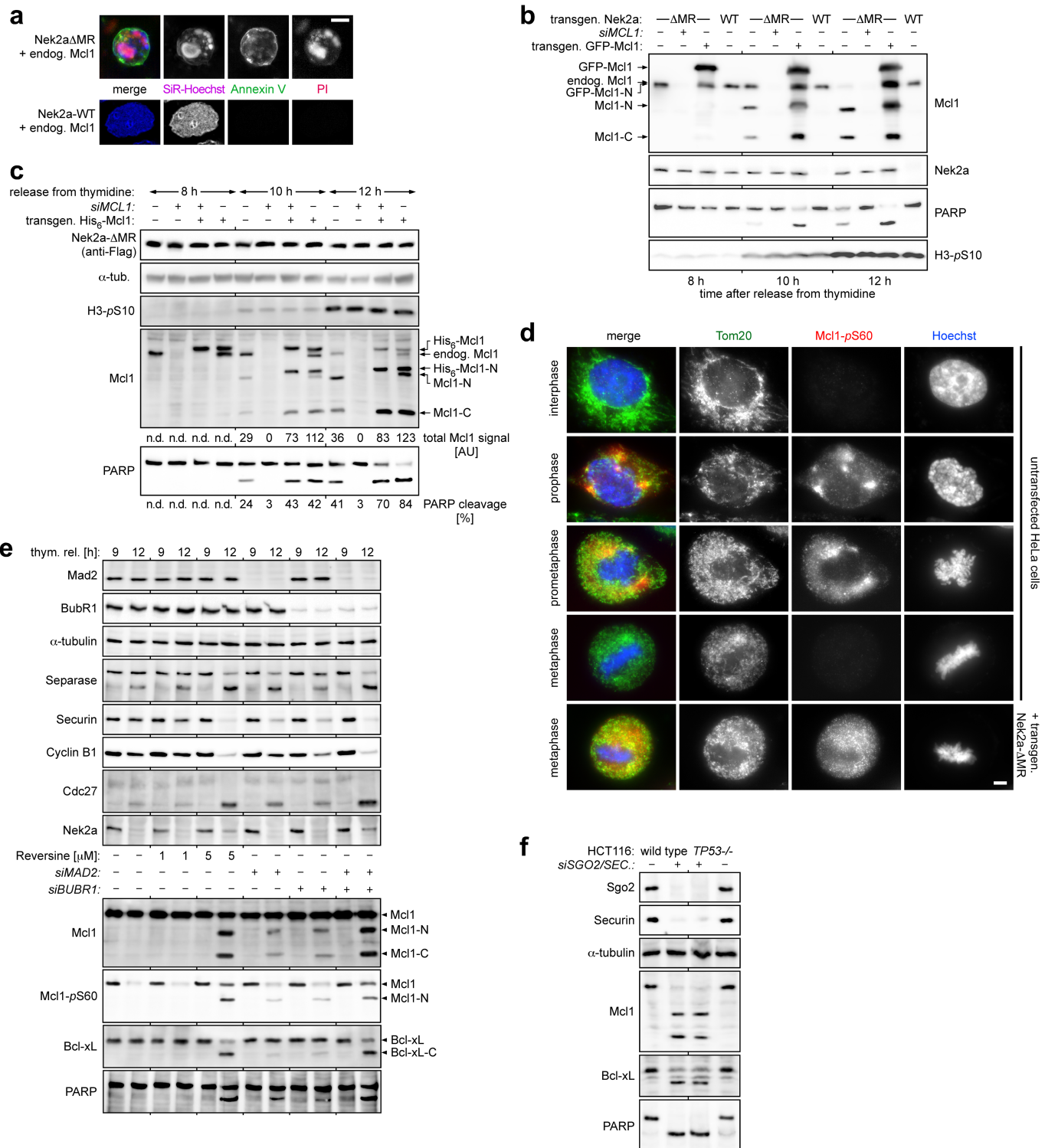


Extended Data Fig. 10 | Stabilized NEK2A and constitutively cleavable MCL1- and BCL-XL variants result in DiM upon activation of separase in anaphase. **a**, Cell fate profiles of HeLa-K cells expressing NEK2A-WT or NEK2A- Δ MR and cultured in the presence of SiR-Hoechst and a fluorogenic caspase 3/7 reporter. **b**, Immunoblots of time-resolved separase and MCL1

immunoprecipitations from NEK2A- Δ MR-expressing or control HeLa-K cells released from taxol arrest by addition of ZM-447439 (ZM) at $t=0$ min.

c, d, HeLa-K cells expressing the indicated variants of MCL1 and BCL-XL were analysed as in **a**. (Dephosphorylated) CDC27 served as a marker for late mitosis.

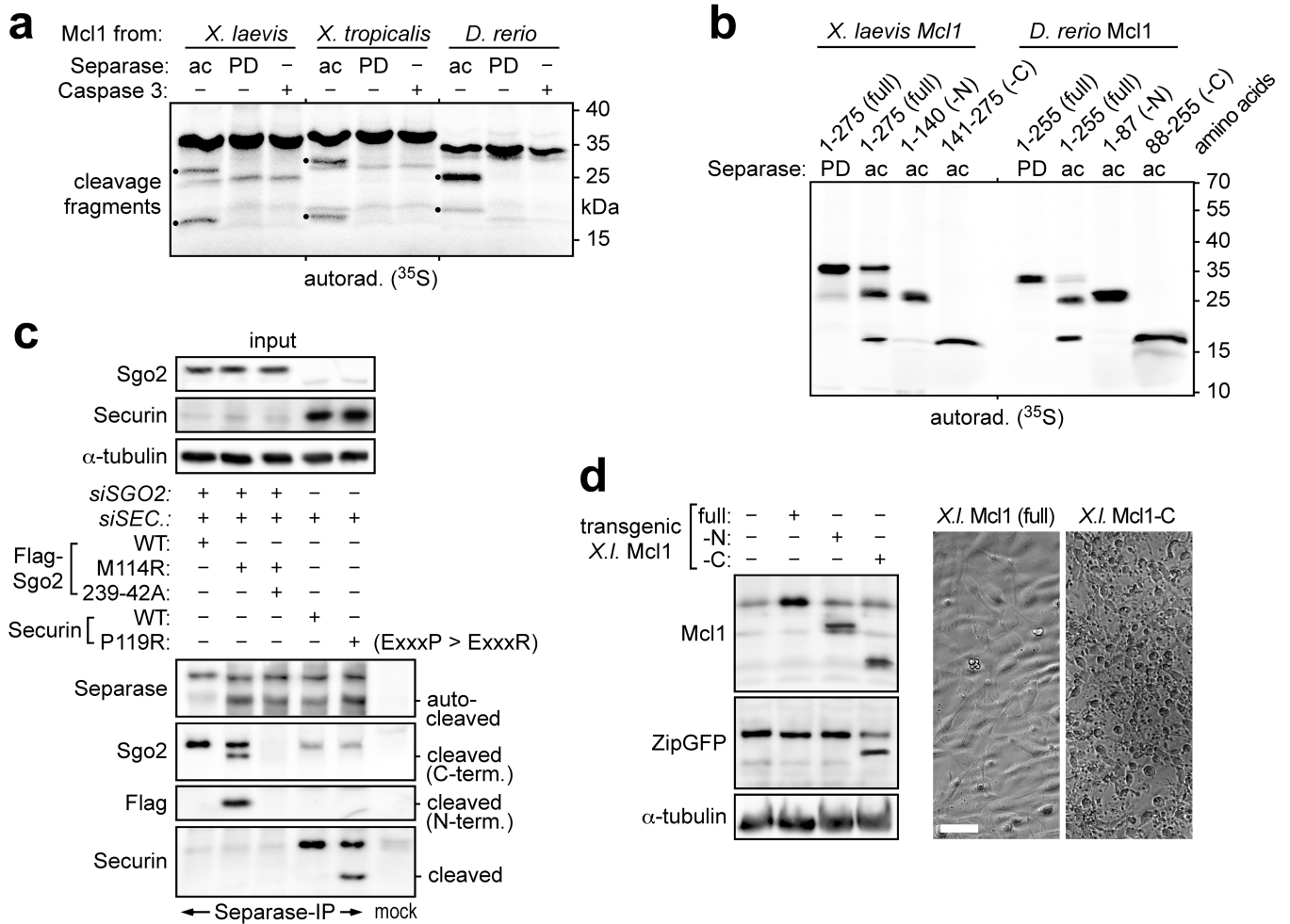
Article



Extended Data Fig. 11 | NEK2A stabilization preferentially kills

MCL1-overexpressing cells. **a, b**, Representative images and immunoblots of quantitative analysis shown in Fig. 4b. Scale bar, 5 μ m. **c**, Immunoblots of NEK2A-ΔMR-expressing Hek293T cells transfected with siMCL1 and expression plasmids for His₆-MCL1 as indicated. Mcl1 and PARP cleavage were quantified densitometrically. n.d., not determined. **d**, MCL1-Ser60 is phosphorylated in early mitosis only. Untransfected or NEK2A-ΔMR-expressing HeLa-K cells were

released from thymidine arrest for 8 h and then analysed by (immuno) fluorescence microscopy using Hoechst and the indicated antibodies. Scale bar, 5 μ m. **e**, Chemical abrogation of the SAC triggers DiM. Immunoblots of reversine- or siRNA-treated HeLa-K cells synchronized as in Fig. 4c. Dephosphorylation of CDC27 into a sharp, fast-migrating band serves as a marker of late mitosis. **f**, TP53^{-/-} cells and parental HCT116 cells were depleted of SGO2 and securin, taxol-arrested and analysed by immunoblotting.



Extended Data Fig. 12 | MCL1 cleavage by separase and the pro-apoptotic effect of MCL1-C is conserved in non-mammalian vertebrates.

a, ^{35}S -labelled, NEK2A/ATP-treated full-length Mcl1 from *X. laevis*, *X. tropicalis* and *D. rerio* were incubated with separase variants and caspase 3 as indicated, and analysed by autoradiography. **b, c**, Separase can cleave after ExxxR motifs. **b**, *X. laevis* and *D. rerio* Mcl1 are cleaved by separase after 136-ExxxR-140 and 84-ExxR-87, respectively. The indicated full-length Mcl1 or fragments thereof

were analysed as in **a, c**. Changing the pseudo-substrate sequence of securin to ExxxR turns it into a separase substrate. Endogenous human SGO2 and securin were depleted by RNAi and replaced by the indicated variants⁹. These were then assessed for cleavage by immunoprecipitation and western blotting.

d, *Xenopus* S3 cells transfected to express ZipGFP and the indicated forms of *X. laevis* Mcl1 were analysed by immunoblotting (left) and video microscopy (representative phase contrast images on right). Scale bar, 50 μm .

Reporting Summary

Nature Research wishes to improve the reproducibility of the work that we publish. This form provides structure for consistency and transparency in reporting. For further information on Nature Research policies, see [Authors & Referees](#) and the [Editorial Policy Checklist](#).

Statistics

For all statistical analyses, confirm that the following items are present in the figure legend, table legend, main text, or Methods section.

n/a Confirmed

- The exact sample size (n) for each experimental group/condition, given as a discrete number and unit of measurement
- A statement on whether measurements were taken from distinct samples or whether the same sample was measured repeatedly
- The statistical test(s) used AND whether they are one- or two-sided
Only common tests should be described solely by name; describe more complex techniques in the Methods section.
- A description of all covariates tested
- A description of any assumptions or corrections, such as tests of normality and adjustment for multiple comparisons
- A full description of the statistical parameters including central tendency (e.g. means) or other basic estimates (e.g. regression coefficient) AND variation (e.g. standard deviation) or associated estimates of uncertainty (e.g. confidence intervals)
- For null hypothesis testing, the test statistic (e.g. F , t , r) with confidence intervals, effect sizes, degrees of freedom and P value noted
Give P values as exact values whenever suitable.
- For Bayesian analysis, information on the choice of priors and Markov chain Monte Carlo settings
- For hierarchical and complex designs, identification of the appropriate level for tests and full reporting of outcomes
- Estimates of effect sizes (e.g. Cohen's d , Pearson's r), indicating how they were calculated

Our web collection on [statistics for biologists](#) contains articles on many of the points above.

Software and code

Policy information about [availability of computer code](#)

Data collection

No commercial open source software was used to collect data.

Data analysis

Because no complex statistical analysis is performed standard analysis programmes (excel 2016, sigma Plot 9.0) were used. Densitometric quantification of western blot signals was done using Multi Gauge (Fujifilm). For FACS data analysis CXP 2.2 software (Beckman Coulter) was used. To handle and edit live cell videos and images LasAF version 2.7.0.9329 (Leica) was utilized. For 2D-SIM image reconstruction ImageJ 1.52i was used.

For manuscripts utilizing custom algorithms or software that are central to the research but not yet described in published literature, software must be made available to editors/reviewers. We strongly encourage code deposition in a community repository (e.g. GitHub). See the Nature Research [guidelines for submitting code & software](#) for further information.

Data

Policy information about [availability of data](#)

All manuscripts must include a [data availability statement](#). This statement should provide the following information, where applicable:

- Accession codes, unique identifiers, or web links for publicly available datasets
- A list of figures that have associated raw data
- A description of any restrictions on data availability

The authors declare that all data supporting the findings of this study are available within the paper and its supplementary information files. If there is reasonable request data can also be provided from the corresponding author.

Field-specific reporting

Please select the one below that is the best fit for your research. If you are not sure, read the appropriate sections before making your selection.

- Life sciences Behavioural & social sciences Ecological, evolutionary & environmental sciences

For a reference copy of the document with all sections, see nature.com/documents/nr-reporting-summary-flat.pdf

Life sciences study design

All studies must disclose on these points even when the disclosure is negative.

Sample size	We did not perform statistical analysis to determine a specific sample size. We used standard cell culture based experiments and minimally reproduced the results in three independent trials using cells from individual cryo-stocks.
Data exclusions	No data were excluded.
Replication	The values obtained from distinct experimental trials were reproducible. The data are presented as means together with the corresponding individual data points from each repetition to indicate biological variation. Experiments analysed by immunoblotting were repeated 2-4 times with similar results (2-4 biological replicates).
Randomization	n/a
Blinding	For quantitative analyses of chromosome spreads and IFM specimen the investigators were blinded to sample allocation.

Reporting for specific materials, systems and methods

We require information from authors about some types of materials, experimental systems and methods used in many studies. Here, indicate whether each material, system or method listed is relevant to your study. If you are not sure if a list item applies to your research, read the appropriate section before selecting a response.

Materials & experimental systems	Methods
n/a <input type="checkbox"/> Involved in the study <input checked="" type="checkbox"/> Antibodies <input type="checkbox"/> Eukaryotic cell lines <input checked="" type="checkbox"/> Palaeontology <input checked="" type="checkbox"/> Animals and other organisms <input checked="" type="checkbox"/> Human research participants <input checked="" type="checkbox"/> Clinical data	n/a <input type="checkbox"/> Involved in the study <input checked="" type="checkbox"/> ChIP-seq <input checked="" type="checkbox"/> Flow cytometry <input checked="" type="checkbox"/> MRI-based neuroimaging

Antibodies

Antibodies used	Rabbit anti-separase (1.5 µg/ml) see Ref. in Material and Methods, mouse anti-Flag M2 (1:2,000; Product No. F1804; Sigma-Aldrich), rabbit anti-Sgo2 (1:1,000; Product No. A301-262A; Lot. No. A301-262A-1; Bethyl), rabbit or guinea pig anti-Sgo2 (1.5 µg/ml; raised by Charles river laboratories against the peptide: DVPPRESHSHSDQSSKC), rabbit anti-Sgo1 (1:500, Abcam ab21633), mouse anti-securin (1:1,000; clone DCS-280; Code No. K009-3; MBL), rabbit anti-phosphoSer10-histone H3 (1:1,000; Product No. 06-570; Lot No. 2370127; Millipore), mouse anti-cyclin B1 (1:1,000; Product No. 05-373; Lot. No. 2199734; Millipore), rabbit anti-Pin1 (1:1,000) see Ref. in Material and Methods, rabbit anti-caspase 3 Asp175 (1:1,000; clone 5A1E; Product No. 9664; Cell Signaling), rabbit anti-Bcl-XL (1:1,000; Product No. 2762; Cell Signaling), mouse anti-Mcl1 (1:800; clone W16014A; Product No. 695702; BioLegend), guinea-pig anti-Mcl1 (1 µg/ml; raised by Charles River Laboratories against bacterially expressed human Mcl1ΔTM), guinea pig anti-phosphoSer10-Mcl1 ('Mcl1-pS60'; 0.5 µg/ml; for IFM 1 µg/ml; anti-CVIGGpSAGA liberated from reactivity towards CVIGGSAGA), rabbit anti-Sororin (1 µg/ml; raised by Charles River Laboratories against bacterially expressed full-length human sororin), rabbit anti-PARP (1:800; clone 46D11; Product No. 9532; Cell Signaling), mouse anti-PARP (1:1,000; clone C-2-10; Product No. AM30; Calbiochem), mouse anti-Tom20 (1:500; Santa-Cruz Biotechnology, F10), mouse anti-cytochrome c (1:1,000; BD Pharmingen, 7H8.2C12), mouse anti-BubR1 (1:1,000; BD Transduction Laboratories, clone 9), rabbit anti-Bax (1:1,000; Abcam, ab32503), rabbit anti-Bak (1:1,000; Abcam, ab32371), rabbit anti-Phosphothreonine (1 µg/ml; Product No. 71-8200; Invitrogen), rabbit anti-Mad2 (1:1,000; Bethyl, A300-300A), anti-MBP monoclonal (1:1,000; NEB Biolabs; HRP-conjugated; Product No. E8032), mouse anti-Nek2 (1:600; clone 20/Nek2 Ruo; Product No. 610593; BD Transduction Laboratories), goat anti-Cdc27 (1:1,000) see Ref. in Material and Methods, mouse anti-RGS-His (1:1,000; Product No. 34610; Qiagen), rabbit anti-phosphoSer139-histone H2A.X (γH2AX; 1:5,000; clone EP854(2)Y; Product No. MABE205; Lot No. 2034733; Millipore), mouse anti-topoisomerase IIα (1:1,000; clone 1C5; Product No. ADI-KAM-CC210-E; Enzo Life Sciences), mouse anti-cyclin A2 (1:200; clone 46B11; Product No. sc-53234; Santa Cruz Biotechnology), rat anti-HA (1:2,000; clone 3F10; Product No. 11867423001; Roche), mouse anti-GFP (hybridoma supernatant 1:2,000; gift from D. van Essen and S. Saccani), and mouse anti-α-tubulin (hybridoma supernatant 1:200; DSHB; clone 12G10), rabbit anti-murine Ptg1 and anti-murine Sgo1 sera (both 1:1,000; gift from Alberto M. Pendas).
-----------------	----------------------------------------------------------------------------------------------------------------------------------------------------------------------------------------------------------------------------------------------------------------------------------------------------------------------------------------------------------------------------------------------------------------------------------------------------------------------------------------------------------------------------------------------------------------------------------------------------------------------------------------------------------------------------------------------------------------------------------------------------------------------------------------------------------------------------------------------------------------------------------------------------------------------------------------------------------------------------------------------------------------------------------------------------------------------------------------------------------------------------------------------------------------------------------------------------------------------------------------------------------------------------------------------------------------------------------------------------------------------------------------------------------------------------------------------------------------------------------------------------------------------------------------------------------------------------------------------------------------------------------------------------------------------------------------------------------------------------------------------------------------------------------------------------------------------------------------------------------------------------------------------------------------------------------------------------------------------------------------------------------------------------------------------------------------------------------------------------------------------------------------------------------------------------------------------------------------------------------------------------------------------------------------------------------------------------------------------------------------------------------------------------------------------------------------------------------------------------------------------------------------------------------------------------------------------------------------------------------------------------------------------------------------------------------------------------------------------------------------------------------------------------------------------------------------------------------------------------

Validation

Validation procedures used for commercial antibodies are described by the manufacturer. Self-made polyclonal rabbit or guinea pig antibodies are validated using multiple methods (e.g. ICC/IF, WB or IP). To address antibody specificity we used the corresponding antigen (e.g. recombinantly expressed in E. coli, IVTT or cell lysate) as positive and siRNA depleted lysate or fixed cells as negative control.

Eukaryotic cell lines

Policy information about [cell lines](#)

Cell line source(s)

Hek293T (Gift from Marc W. Kirschner); HeLa-K (Gift from Thomas U. Mayer); RPE-1 hTERT (ATCC, CRL-4000); HCT116 parental and Bak/Bax DKO (Gift from Richard Joule); SW480, T47D, A427 and A549 (Gift of Michael Orth from); NIH3T3 purchased from ATCC (CRL-1658); TP53 KO (Gift from Bert Vogelstein); Xenopus laevis S3 (Gift from Guowei Fang)

Authentication

Cell were authenticated via visual inspection of typical morphology, by immunoblotting analyses and cell synchronization behavior, and through selective resistance to antibiotic treatments.

Mycoplasma contamination

Cell lines were not tested for mycoplasma contamination but microscopic inspections of their fluorescently labeled DNA contents were inconspicuous.

Commonly misidentified lines

(See [ICLAC](#) register)

No commonly misidentified cell lines were used.